nature communications

Article

https://doi.org/10.1038/s41467-025-64792-2

Optimizing carbon footprint in long-haul heavy-duty E-Truck transportation

Received: 15 October 2024

Accepted: 25 September 2025

Published online: 29 October 2025

Check for updates

Junyan Su [1], Qiulin Lin [1] & Minghua Chen [1,2]

Electrifying heavy-duty trucks is crucial for decarbonizing transportation, but maximizing their potential requires minimizing the carbon footprint of timely deliveries. This complex optimization task involves strategic path, speed, and charging planning, which traditional methods struggle to optimize at scale. We present a stage-expanded graph formulation that reduces complexity and reveals a useful problem structure. Our formulation naturally decomposes the problem into more tractable subproblems, allowing efficient coordination between routing and charging decisions, and maintains a manageable graph size. We exploit these structural insights to design an efficient algorithm with performance guarantees. Simulations using real-world data over the U.S. highway system demonstrate that our method complements the 36% carbon reduction from electrification with an additional 25% decrease, totaling a 61% reduction. Moreover, our carbon-optimized strategy, applicable to various truck types, can achieve comparable carbon reductions 9 years sooner than zero-emission truck adoption alone. This approach accelerates transportation decarbonization, offering a powerful tool in the fight against climate change.

Climate change is the defining crisis of our time, and it is tied to the rising anthropogenic greenhouse gas (GHG) emissions. Reducing or even eliminating the GHG emissions across all major sectors is critical to meet the 1.5 °C climate target. In the U.S., the transportation sector has become the largest source of GHG emissions, accounting for 37% of the country's total carbon dioxide (CO_2, the primary anthropogenic GHG) emissions[1]. With only 0.4% of the total on-road vehicle population, long-haul heavy-duty trucks are responsible for 11% of transportation carbon emissions (cf. Supplementary Fig. 1 in Supplementary Information Section 4). Decarbonizing long-haul heavy-duty trucks, i.e., reducing CO_2 and other GHG emissions from their operations, is thus a disproportionately high leverage point in the scope of the climate change mitigation framework.

Electrifying long-haul heavy-duty trucks is a critical step towards decarbonizing the trucking sector[2]. Electric trucks (E-Trucks) not only enhance the driving experience with their rapid acceleration and quieter operation but also eliminate tailpipe emissions and offer a potential to reduce carbon emissions[3]. Along this line, the U.S. government has set a target to electrify 30% of medium- and heavy-duty truck sales by 2030 and 100% by 2040[4]. However, achieving E-Trucks' full decarbonization potential requires not only fast E-Truck adoption but also a careful consideration of how they are operated and charged, as the charging electricity incurs carbon footprints—the carbon emissions during electricity generation. For clarity and brevity in our discussion, we assume all references to trucks pertain to long-haul heavy-duty models unless specified otherwise.

We argue that the full decarbonization potential of E-Trucks is jeopardized by the current common practice of driving as quickly as possible along the shortest path. Such driving practice often underutilizes the geographical information and the traffic information, resulting in inefficient paths and speed plans that consume substantial energy[5]. Moreover, the current practice of charging E-Trucks—charging whenever the battery level falls below a certain threshold—often fails to consider the source of electricity, using gray electricity with higher carbon intensity—the amount of carbon emissions per unit of electricity during generation. Depending on different mixes of electricity generation (cf. Table 1), the carbon intensity presents large geospatial and temporal fluctuations due to the inherent intermittency

[1]Department of Data Science, City University of Hong Kong, Hong Kong, China. [2]School of Data Science, The Chinese University of Hong Kong, Shenzhen, Guangdong, China. e-mail: minghua@cuhk.edu.cn

of renewable energy sources, as illustrated in Fig. 1. Ignoring such spatial-temporal diversity of carbon intensity may lead to a large carbon footprint during charging. Indeed, as suggested by our numerical studies with real-world data over the U.S. highway system, common practice operations could under-realize E-Truck's decarbonization potential by 25%. Even worse, improper charging and operation of E-Trucks might even lead to a higher carbon footprint than ICE trucks; see Supplementary Section 5.2 for an example of inefficient E-Truck operation and Supplementary Section 5.3 for an example of carbon-optimized operation. It is thus essential to optimize the truck operations to unleash E-Trucks' full decarbonization potential.

In this paper, we study the problem of minimizing the carbon footprint of long-haul heavy-duty E-Trucks' timely transportation, a critical operation module. This involves strategically orchestrating path planning, speed planning, and intermediary charging planning as E-Trucks navigate national highway networks within tight delivery timeframes. The path planning and speed planning jointly optimize the E-Truck's energy efficiency by selecting the most effective routes and maintaining optimal speeds. Meanwhile, the charging planning strategically schedules charging sessions and locations to utilize clean electricity with low carbon intensity. Such a carbon footprint optimization (CFO) problem is essential for realizing the environmental advantages of E-Trucks. However, it remains intractable due to a combination of challenges: (i) the strict delivery deadline, (ii) the battery operational constraints, (iii) the non-convexity of the objective function, and (iv) the enormous search space of charging decisions across a vast network with diverse carbon intensity profiles. Indeed, the CFO problem is NP-hard and more complicated and challenging than those in related studies for internal combustion engine (ICE) truck[5,6] and electric vehicle (EV) driving optimization[7–9]. Existing mathematical models (cf. Supplementary Table 2 in Supplementary Information Section 2) and approaches (cf. Supplementary Table 3 in Supplementary Information Section 3) either do not apply to the problem or fail to solve the problem effectively, especially for large-scale instances; see Supplementary Section 2 for a more detailed discussion of the related work.

To address this challenging problem, we propose a stage-expanded graph formulation, which transforms the CFO problem into a Generalized Restricted Shortest Path (GRSP) problem[5,10] under practical settings. The key advantages of this formulation are its low model complexity and the exposure of a problem structure that facilitates efficient algorithm design. By exploiting this structure, we devise a dual-subgradient algorithm that is provably convergent. We show that each iteration of this algorithm runs in polynomial time relative to the network size. We also establish a sufficient condition for optimality and derive a posterior bound on the solution quality when this condition is not satisfied. Furthermore, our mathematical formulation and approach are general and extendable to other long-haul heavy-duty trucks, including hydrogen fuel cell electric trucks (FCE-Trucks), and ICE trucks. Our algorithm demonstrates strong empirical performance in extensive simulations conducted with real-world data, enabling a thorough evaluation of the decarbonization potential of E-Trucks in realistic operational settings.

Using our solution as a building block, we evaluate the full decarbonization potential of E-Trucks and the benefits of carbon-optimized operations. We conduct extensive simulations over the US national highway network with the real-world data. We highlight the following key findings: (i) With common practice operation, the E-Truck achieves a 36% carbon reduction compared to the conventional ICE trucks, validating the decarbonization potential of E-Trucks. (ii) Our carbon-optimized operation achieves an extra carbon reduction of 25%, of which the carbon-aware charging and energy-efficient driving contribute 12% and 13%, respectively. The aggregate 61% carbon reduction of the U.S. long-haul trucking sector amounts to 2.4% of the total U.S. carbon emissions, or approximately the entire carbon footprint of countries like Qatar[11]. (iii) The carbon-optimized operations, when applied to ICE trucks, FCE-Trucks, and E-Trucks, accelerate the decarbonization progress, achieving the same level of carbon reduction 9 years sooner than relying solely on adopting zero-emission trucks. With the deployment of carbon-optimized operations, the whole long-haul trucking sector will achieve a substantial carbon reduction by 2050−62% reduction relative to 2019 levels with BAU projection, of which the adoption of zero-emission trucks contributes 5%, carbon-optimized operations contribute 31%, and grid decarbonization contributes 26%.

Table 1 | The U.S. electricity generation and resulting CO_2 emissions of major types of energy source in 2020 [64, Table 7.2a, Table 11.6]

	Coal	Natural Gas	Petroleum	Renewable
Carbon Intensity (kg/kWh)	1.02	0.39	0.91	0
Total Emission (tons)	7.86×10^{8}	6.35×10^{8}	1.6×10^{7}	0
Electricity (kWh)	7.73×10^{11}	1.62×10^{12}	1.75×10^{10}	7.92×10^{11}

Different energy source has different carbon intensity.

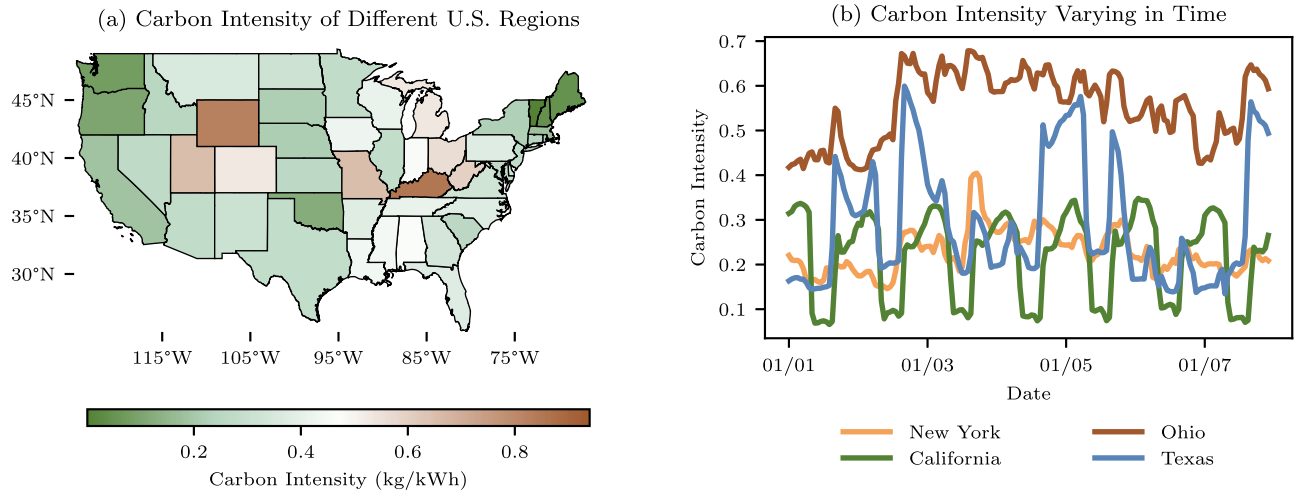

Fig. 1 | Spatial-temporal diversity of the U.S. carbon intensity (kg/kWh). a The average carbon intensity in different states. **b** The carbon intensity varying in time during the first week of 2024[15]. Large variation in carbon intensity are commonly observed in other times of the year. Source data of this figure are provided in the Source Data file.

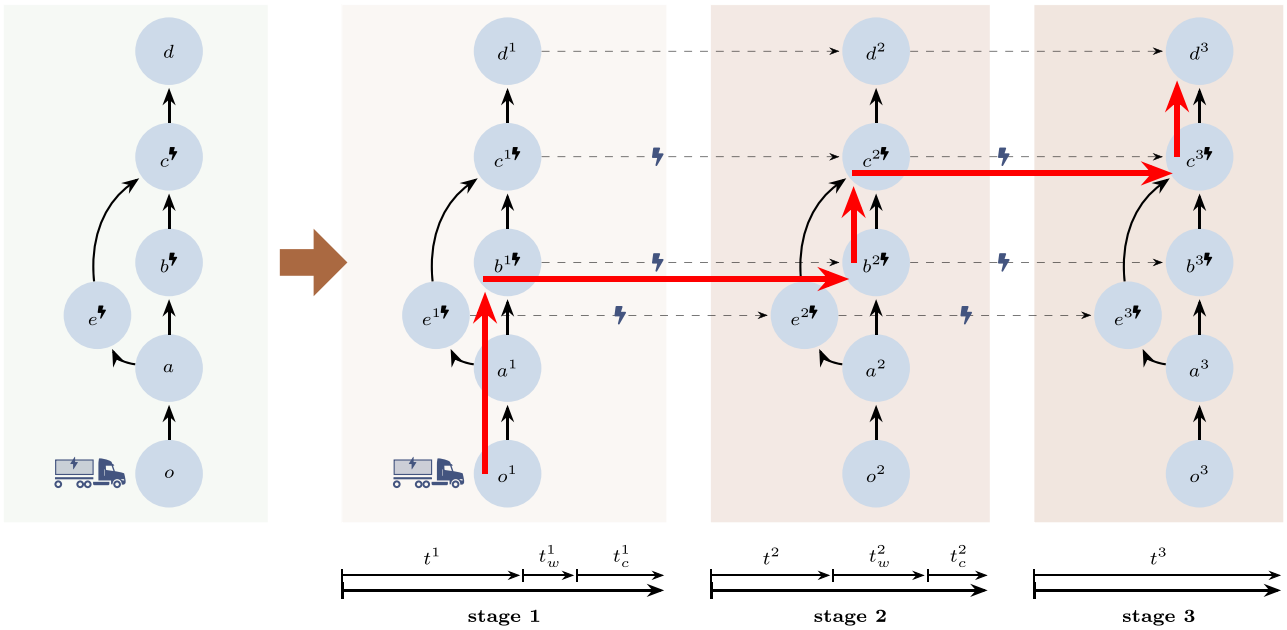

Fig. 2 | Illustration of a stage-expanded graph for an E-Truck timely transportation task with $N = 2$ charging stops. Nodes b, c, and e represent charging stations within the original transportation network. The red path indicates a feasible operation candidate for an E-Truck traveling from origin o^1 to destination d^3. The constructed stage-expanded graph comprises $N+1=3$ stages. In the first stage, the E-Truck travels from o^1 to b^1, with a travel time t^1, then waits for t_w^1 amount of time and charges at b^1 for t_c^2 amount of time. Subsequent stages involve similar sequences of travel, waiting, and charging. Dashed arrows represent virtual edges that denote potential charging decisions between consecutive stages.

Paper Outline. We begin by presenting the problem formulation and our methodology, emphasizing key technical innovations and contributions. We then demonstrate through comprehensive numerical experiments the decarbonization potential achievable through our integrated approach, providing quantitative insights into system-wide emissions reductions and operational efficiency gains. We conclude the main text with a assessment of current limitations and promising avenues for future research in "Discussion". Complete methodological details and algorithmic frameworks are presented in Methods, with additional supporting analyses, extended data tables, and supplementary figures provided in the accompanying Supplementary Information.

Results

An efficient approach for carbon-optimized E-Truck timely transportation

We first introduce essential notations and the problem setting, followed by an overview of the key ideas underpinning our approach. Detailed discussions on the model and algorithm are deferred to Methods. We model the highway system as a directed graph $\mathcal{G}=(\mathcal{V},\mathcal{E})$. The node set $\mathcal{V}=\mathcal{V}_r\cup\mathcal{V}_c$ consists of road nodes $\mathcal{V}_r$ (representing segment endpoints) and charging stations $\mathcal{V}_c$. The edge set $\mathcal{E}\subset\mathcal{V}\times\mathcal{V}$ represents road segments. We consider an E-Truck traveling from an origin $o\in\mathcal{V}$ to a destination $d\in\mathcal{V}$ within a hard deadline T. The objective is to minimize the carbon footprint of the electricity used along this trip. The E-Truck has a battery capacity B and needs to maintain a positive battery State-of-Charge (SoC) throughout the trip. We consider the E-Truck begins the journey with an initial battery SoC $\beta_0\in[0,B]$. The solution to the problem includes (i) the path plan: a sequence of edges from o to d; (ii) the speed plan: a speed profile across these edges; (iii) the charging plan: the selection of intermediary charging stations, along with wait and charge times at each selected charging station.

One of our key methodological contributions is the stage-expanded graph, a construction that extends $\mathcal{G}$ to integrate charging decisions. The stage-expanded graph originates from the following key observations: (i) in practice, an E-Truck operator only charges for a small number of times during a trip, e.g., 3–4 times charging for a 1500-mile E-Truck transportation; (ii) the truck operation between two consecutive charging stops (a stage) reduces to an energy-efficient driving problem for which efficient algorithms are available[5,6]; (iii) given the truck operations at each stage, the carbon-aware charging decisions between each two consecutive stages become tractable to optimize.

Given these observations, we construct the stage-expanded graph $\mathcal{G}_s=(\mathcal{V}_s,\mathcal{E}_s)$ as follows. We assume the E-Truck can make up to N charging stops along its trip, where N is a parameter provided to the problem. The graph $\mathcal{G}_s$ consists of $N+1$ stages, corresponding to the $N+1$ segments of the journey between charging events. The node set $\mathcal{V}_s$ is composed of $N+1$ copies (one copy for each stage) of the original nodes in $\mathcal{V}$: $\mathcal{V}_s=\{v^i : v\in\mathcal{V}, i\in\{1,\ldots,N+1\}\}$. The edge set $\mathcal{E}_s$ contains (i) the original edges replicated across all stages, and (ii) virtual edges connecting the same charging stations and the destination between consecutive stages. Formally, we define:

$$\begin{aligned}\mathcal{E}_{s1} &= \{(u^i,v^i) : (u,v)\in\mathcal{E}, i\in\{1,\ldots,N+1\}\},\\ \mathcal{E}_{s2} &= \{(v^i,v^{i+1}) : v\in\mathcal{V}_c\cup\{d\}, i\in\{1,\ldots,N\}\},\\ \text{and } \mathcal{E}_s &= \mathcal{E}_{s1}\cup\mathcal{E}_{s2}.\end{aligned}\tag{1}$$

When an E-Truck, at stage i, arrives at a charging station $v\in\mathcal{V}_c$, it can choose to end the current stage and charge. This action is represented by traversing the charging edge (v^i,v^{i+1}). Within each stage, the E-Truck needs to travel towards the next charging station or the final destination. Upon arrival, it can charge at the charging station and advance to the next stage or, if at the destination, end its journey. Note that the E-Truck can charge for less than N times, arrive at the destination at stage $i<N+1$, and then travel across stages through virtual edges until reaching the final stage, mimicking waiting at the destination upon early arrival. We provide an illustration of the stage-expanded graph in Fig. 2.

The stage-expanded graph captures the problem structure and decomposes the routing and charging decisions. Specifically, we can

https://doi.org/10.1038/s41467-025-64792-2

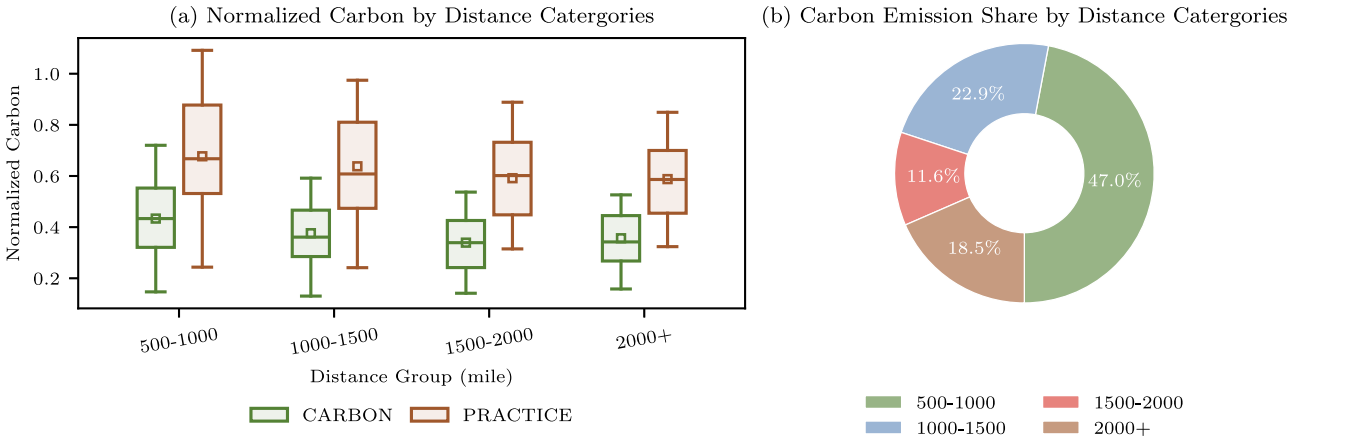

Fig. 3 | The normalized carbon footprint under different driving strategies and the carbon emission shares by different distance categories. a The normalized carbon footprint for electric trucks relative to ICE Trucks across distance categories. Results compare carbon-optimized operations (CARBON) with conventional baseline operations (PRACTICE). Box plots show interquartile ranges (25th–75th percentiles) with median values indicated by internal lines. Square markers denote mean values, and error bars represent ±1.5 standard deviations. **b** The estimated carbon emission share of distance category for long-haul heavy-duty trucks (data from NREL[14]). Source data of this figure are provided in the Source Data file.

separately optimize the energy-efficient timely transportation subproblem within each stage and the carbon-aware charging subproblem between stages, followed by a higher level of coordination for the solutions of the subproblems. Those subproblems are more tractable than the original CFO problem. Efficient algorithms are available for the energy-efficient timely transportation subproblems[5,6], and the size of the carbon-aware charging subproblems is small. Moreover, the revealed structure comes with a minor increase in graph size—the size of the stage-expanded graph is only $N+1$ times the original graph, where the number of charging stops N is a small constant in practice. This is in sharp contrast to the time-expanded graph[8] or the battery-expanded graph[12], which substantially increase the graph size as discussed in Supplementary Table 3 in Supplementary Information Section 3. We explore the problem structure and formulate the CFO problem as a GRSP problem on the stage-expanded graph. We then propose an efficient dual-based algorithm, which features guaranteed convergence and polynomial complexity per iteration. We also establish a sufficient condition for optimality and derive a posterior bound on the solution quality when this condition does not hold. Besides the favorable theoretical properties, our algorithm demonstrates strong empirical performance, allowing us to examine the full benefits of E-Truck decarbonization using real-world data. See "Methods" for our formal problem formulation, algorithm design, and performance analysis. See also Supplementary Section 3 for a remark on the novelty of our approach and a comparison with conceivable alternatives.

Numerical experiment setup

To evaluate the decarbonization potential of truck electrification and the enhanced environmental benefits of carbon-optimized E-Truck operations, we conduct the simulation on the U.S. highway network with real-world traces. The constructed transportation network contains 84,504 nodes and 178,238 edges. We conduct simulations on long-haul origin-destination pairs from Freight Analysis Framework[13]. We divide the long-haul origin-destination pairs into the four distance categories: 500–1000 miles, 1000–1500 miles, 1500–2000 miles, and 2000+ miles. We then select the top 100 pairs based on freight value from each group, resulting in a total of 400 origin-destination pairs. More details of the simulation setup can be found in Methods.

In the following, we will present the key findings focusing on the implications of carbon-optimized operations for the truck decarbonization strategies. More supplementary simulation results can be found in the Supplementary Information, including (i) the applicability of our approach to timely heavy-duty truck transportation over the European continent highway system (Supplementary Section 7), (ii) the robustness analysis of our approach (Supplementary Section 8.2), and (iii) the runtime performance of our approach and other alternatives (Supplementary Section 8.4 and Supplementary Section 8.3).

Truck electrification reduces carbon emissions

We first evaluate the decarbonization potential of truck electrification alone in reducing carbon emissions. In the following, we use the ICE truck, operated with common practice that drives on the fastest path at top truck speeds, as the baseline. We then compare the ICE truck with the E-Truck operated with a conceivable baseline that mimics the common practice (denoted by PRACTICE), which drives on the fastest path also at top truck speeds, and charges whenever the battery level falls below a certain threshold. For each origin-destination pair, we compute the normalized carbon footprint of the E-Truck with respect to the ICE truck and present the results in Fig. 3. We find that under the PRACTICE baseline, the average normalized carbon footprints of the E-Truck are 0.69, 0.61, 0.59, and 0.59 for the four distance categories, respectively. Those numbers, combined with the estimated carbon share of different distance categories for long-haul heavy-duty trucks[14], indicate that the E-Truck can achieve an average reduction of 36% of carbon emissions compared to traditional ICE trucks—a testament to the decarbonization potential of truck electrification. This potential, however, remains underexplored due to inefficient operations. The normalized carbon footprint varies largely across different origin-destination pairs, revealing room for optimization. More concerning, improper operation can actually result in the E-Truck producing a higher carbon footprint than its ICE counterpart, as illustrated in Supplementary Section 5.2. This operational inefficiency underscores the importance of optimized operations in maximizing the decarbonization potential of E-Trucks, which we elaborate on in the following analysis.

Carbon-optimized timely transportation maximizes E-Truck decarbonization potential

We then study the full decarbonization potential of E-Trucks by our carbon-optimized operations (denoted by CARBON). We run our approach over the same set of origin-destination pairs and compare the performance of CARBON with the PRACTICE baseline. As demonstrated in Fig. 3, we find that the average normalized carbon footprint of CARBON are 0.43, 0.37, 0.34, and 0.35 for the four distance

https://doi.org/10.1038/s41467-025-64792-2

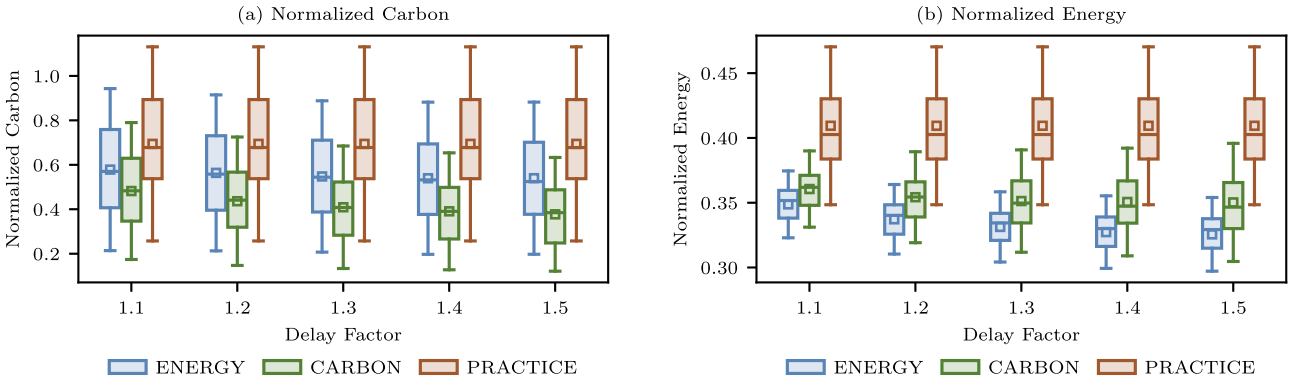

Fig. 4 | Carbon footprint and energy consumption of E-Trucks under different operations with different delay factors. A larger delay factor means a more relaxed deadline. The results are for the distance category of 500–1000 miles. The results for all four distance categories can be found at Supplementary Fig. 7 in Supplementary Information Section 6.2. **a** The normalized carbon footprint with respect to ICE trucks under today's common practice. **b** The normalized energy consumption with respect to ICE trucks under common practice. In both (**a**, **b**), box plots show interquartile ranges (25th–75th percentiles) with median values indicated by internal lines. Square markers denote mean values, and error bars represent ±1.5 standard deviations. Source data of this figure are provided in the Source Data file.

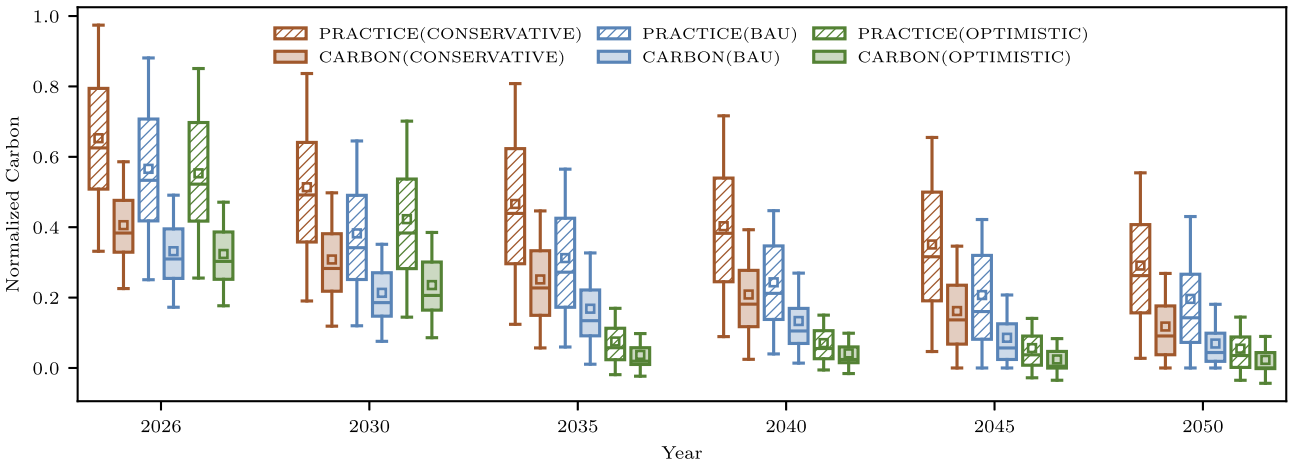

Fig. 5 | Normalized carbon emissions of electric trucks relative to internal combustion engine trucks. We compare carbon-optimized operation (CARBON) with common practice operation (PRACTICE) across different grid decarbonization scenarios: business-as-usual (BAU), conservative projection (CONSERVATIVE), and optimistic projection (OPTIMISTIC). Box plots show interquartile ranges (25th–75th percentiles) with median values indicated by internal lines. Square markers denote mean values, and error bars represent ±1.5 standard deviations. The mean values, median values, and standard deviations are weighted by emission share in each distance category. Source data of this figure are provided in the Source Data file.

categories, respectively, leading to a weighted average of 0.39 compared to the ICE truck. These results show that, carbon-optimized operations achieve an additional 25% carbon reduction on top of electrification alone, yielding a cumulative 61% carbon reduction when compared to ICE trucks. The cumulative carbon reduction achieved in the long-haul heavy-duty trucking sector amounts to 2.4% of the total US carbon emissions or approximately the total carbon emissions of countries like the Qatar. Moreover, such reduction is more consistent across different origin-destination pairs than the PRACTICE baseline with a smaller standard deviation in Fig. 3.

We then study the attribution of the carbon reduction from carbon-optimized timely transportation. Recall that the carbon-optimized operations reduce carbon footprint by jointly optimizing: (i) energy-efficient driving by path and speed planning and (ii) carbon-aware charging by charging planning. To further understand the attribution of those two modules, we consider a modified approach (denoted by ENERGY) from our method that uses uniformly constant carbon intensity. The ENERGY baseline isolates the first mechanism by focusing exclusively on energy-efficient driving while deliberately excluding carbon-aware charging considerations. Therefore, by contrasting CARBON and ENERGY results, we isolate and quantify the impact of the second module and specifically demonstrate the significance of carbon-aware charging operations in overall decarbonization performance. We also explore the effects of extending the delivery deadlines on the carbon footprint of E-Trucks by adjusting the deadlines from $1.1T_f$ to $1.5T_f$, where T_f represents the minimum travel time determined by a fastest-path approach detailed in Methods. The ratio T/T_f is referred to as the delay factor. For ease of presentation, we present the results in Fig. 4 for the distance category of 500–1000 miles, which contributes the most carbon share among all distance categories, as seen in Fig. 3. The full results for all distance categories can be found in Supplementary Fig. 7 in Supplementary Information Section 6.2 which demonstrate similar results. We observe that carbon-optimized operations consistently reduce more carbon than energy-efficient ones across various delay factors. For example, at a delay factor of 1.2, carbon-optimized operations achieve an additional 0.12 normalized carbon savings over energy-efficient operations. Therefore, at least 12% out of the 25% additional carbon reduction from the carbon-optimized operation is attributed to carbon-aware charging. These findings, combined with the facts that CARBON consume at most 2.4% more normalized energy on average than ENERGY (cf. Fig. 4b), demonstrate that carbon-optimized timely

https://doi.org/10.1038/s41467-025-64792-2

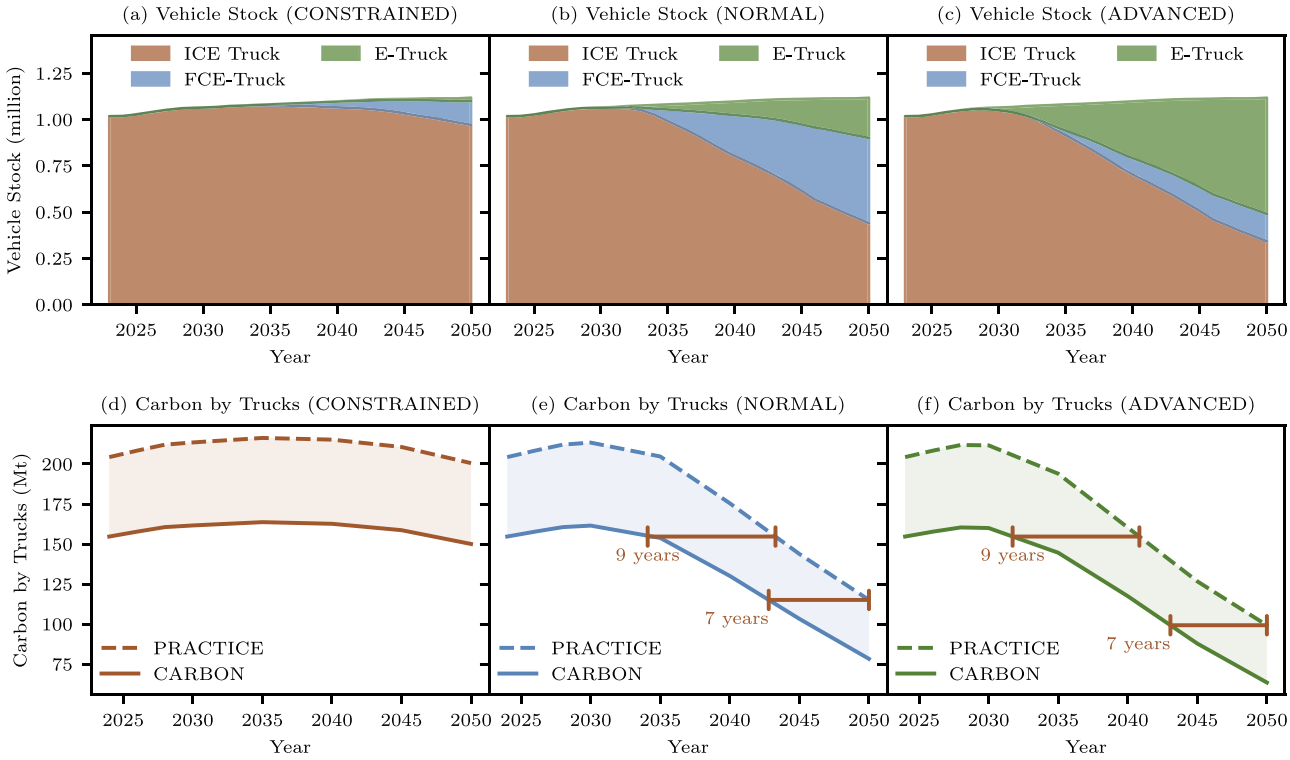

Fig. 6 | The stock share and carbon footprint of long-haul heavy-duty trucks from 2019 to 2050 under different ZEV adoption scenarios. a, **b**, **c** present the stock share for ICE Truck, E-Truck, and FCE-Truck in CONSTRAINED, NORMAL, and ADVANCED ZEV adoption scenarios. **d**, **e**, **f** present the carbon footprint of major types of long-haul heavy-duty trucks, including ICE trucks, FCE-Trucks, and E-Trucks. The solid lines represent the carbon footprint of trucks with common practice (PRACTICE), and the dashed lines represent the carbon footprint of trucks with carbon-optimized operations (CARBON). The shaded areas represent the carbon reduction from carbon-optimized operations compared to common practice. We assume the grid decarbonization scenario to be BAU in this analysis. Source data of this figure are provided in the Source Data file.

transportation simultaneously reduces energy consumption and the carbon footprint via energy-efficient driving and carbon-aware charging, maximizing the environmental benefits brought by E-Trucks.

Carbon-optimized timely transportation boosts truck decarbonization in the future

We then study how carbon-optimized timely transportation reshapes the truck decarbonization pathway in the future, using carbon intensity projection data from the Cambium dataset[15]. This is to examine the usefulness of our approach in different projected carbon intensity settings. We focus on three power grid decarbonization scenarios: (i) Business-As-Usual (BAU) that assumes a continuation of current policies and trends. (ii) CONSERVATIVE that assumes high future costs for renewable investments; (iii) OPTIMISTIC that achieves the full grid decarbonization target by 2035[16] where national-wide carbon intensity is zero, albeit regional ones can fluctuate around zero over time. Negative carbon intensity is achieved by assuming the fast development of nascent technologies[17] like bioenergy with carbon capture and storage (BECSS)[18]. In the following, all carbon reductions are computed by considering the carbon shares of different distance categories shown in Fig. 3.

We commence our investigation by examining the impacts of carbon-optimized operations on a single E-Truck. Our results, presented in Fig. 5, reveal that CARBON achieves an additional carbon reduction of 13% by 2050 in the BAU scenario when compared to the PRACTICE baseline. This additional carbon reduction increases to 17% in the CONSERVATIVE scenario. Even in the OPTIMISTIC scenario, our carbon-optimized solution can still achieve an additional 3% carbon reduction compared to the PRACTICE baseline, by exploiting the (small) fluctuation of carbon intensity over different regions and times.

We further evaluate the impact of carbon-optimized operations across the entire long-haul heavy-duty trucking sector. We examine the major types of long-haul heavy-duty trucks, including ICE trucks, fuel cell electric trucks (FCE-Trucks), and battery electric trucks (E-Trucks). We utilize zero-emission vehicle (ZEV, including FCE-Trucks and E-Trucks) adoption projection data from ref. 14, focusing on the following scenarios: (i) NORMAL that reflects a central set of assumptions; (ii) ADVANCED with lower charging infrastructure cost; (iii) CONSTRAINED with constrained ZEV technology advancement. We tailor our approach in Methods and deploy it to the entire spectrum of long-haul heavy-duty trucks; see Methods for detailed descriptions of such adoption.

Our results also indicate that carbon-optimized timely transportation can contribute to the decarbonization of the trucking sector by reducing carbon emissions more efficiently. In Fig. 6, we observe that there will be an immediate carbon reduction in 2026 by implementing our carbon-optimized operations for ICE trucks, a goal that would otherwise take 9 additional years through ZEV adoption alone. Moreover, carbon reductions achievable by 2050 through ZEV adoption are reached 7 years earlier with carbon-optimized operations. This trend persists under the ADVANCED ZEV adoption scenario. Carbon-optimized operations consistently contribute to trucking sector decarbonization over time. From 2026 to 2030, total emissions increase slightly due to the growing number of trucks, but the subsequent adoption of ZEVs combined with carbon-optimized operations leads to a sharp decline, with a carbon reduction of 62% by 2050, of which ZEV adoption contributes 5% carbon-optimized operations contribute 31%, and grid decarbonization contributes 26% (cf. Fig. 7). Cumulatively, carbon-optimized operations account for an additional CO2 reduction of 1.2 billion tons from 2026 to 2050 compared to common practices.

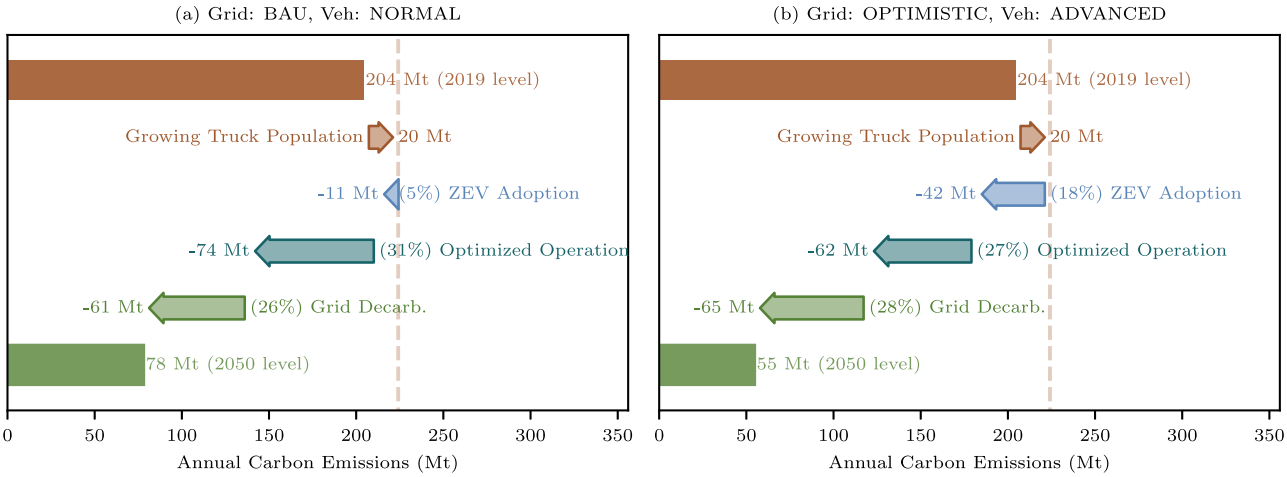

Fig. 7 | The attribution of carbon reductions of 2050 relative to the 2019 level. The carbon emissions increase due to the growing truck population and decrease due to ZEV adoption, carbon-optimized operations, and grid decarbonization, respectively. **a** The attribution under the BAU grid decarbonization scenario and the NORMAL ZEV adoption scenario. **b** The attribution under the OPTIMISTIC grid decarbonization scenario and ADVANCED ZEV adoption scenario.

Discussion

In this paper, we explore how to unlock the full decarbonization potential of long-haul heavy-duty E-Trucks via carbon-optimized timely transportation. We present a stage-expanded graph based problem formulation and an efficient algorithm with favorable theoretical and empirical performance. Through extensive simulations with real-world traces, we show that carbon-optimized operation further reduces the carbon footprint of E-Trucks by 25%, on top of the 36% reduction from electrification alone. The cumulative 61% carbon reduction achieved is comparable to the total carbon footprint of countries like the Qatar. Our approach is applicable to various types of trucks, including ICE and ZEV trucks, allowing us to assess the impact of carbon-optimized operations on the entire spectrum of the trucking industry. Our forward-looking projections suggest that carbon-optimized operations propel truck decarbonization, achieving comparable carbon reduction 9 years earlier than ZEV truck adoption alone.

Operationalizing our approach necessitates a comprehensive software ecosystem capable of driver interaction, real-time data integration, and dynamic optimization of charging, routing, and speed planning. Our framework requires two distinct data categories with varying update frequencies and accessibility characteristics. Static Data encompasses information requiring infrequent updates due to its stable nature: (i) Transportation Network Data, including detailed road mappings, segment-specific grade profiles, and charging station locations; and (ii) Vehicle Specifications, encompassing battery charging characteristics, vehicle weight parameters, and energy efficiency profiles. This data is predominantly accessible through established sources, including OpenStreetMap[19] for transportation networks and manufacturer databases for vehicle specifications. Dynamic Data requires continuous updates to capture real-time operational conditions: (i) Traffic Conditions, providing current congestion levels across road segments; (ii) Charging Infrastructure Status, including real-time availability and queuing times at charging stations; and (iii) Grid Carbon Intensity, reflecting the temporal and spatial variability of electricity generation carbon footprints based on dynamic energy mix compositions. These data streams are accessible through established platforms including transportation APIs[20], charging network platforms[21,22], and grid monitoring systems[23].

While individual data sources exist, successful integration requires developing unified interfaces ensuring compatibility, accuracy, and reliability across heterogeneous systems–necessitating coordinated stakeholder collaboration. Successful deployment demands multi-stakeholder coordination among policymakers, transportation authorities, logistics operators, and energy providers (including grid operators and charging infrastructure companies). Policymakers must establish standardized data interchange protocols, incentivize cross-sector data sharing, and support digital infrastructure investments. Transportation authorities should provide comprehensive road network data and real-time traffic information. Energy providers must deliver accurate, timely data on charging availability and grid carbon intensity. Logistics companies must adopt integrated technological solutions and participate in real-world validation studies. This collaborative ecosystem is essential for realizing the framework's full decarbonization potential in operational environments.

Remarkably, deploying this software ecosystem requires no investment in hardware infrastructure, instead building upon purely algorithmic development and existing data sources. This characteristic enables immediate deployment across existing fleet operations, without the decade-long infrastructure development cycles that typically constrain decarbonization efforts. Our framework thus offers an agile and cost-effective strategy for a rapid decarbonization pathway in the trucking sector.

Beyond long-haul heavy-duty trucks, our approach may not be directly applicable to the operations of light-duty vehicles or short-haul trucks, as their operation settings often involve frequent pickup-delivery scheduling, which is absent in the long-haul heavy-duty vehicle operation studied in this paper[24,25]. However, in cases with long transportation distances and fixed pickup-delivery schedules, our approaches can be applied to minimize their carbon footprint, energy consumption, or monetary cost. Developing general carbon-optimized operation strategies for light-duty vehicles and short-haul trucks deserves further investigation[26,27].

Methods

Our preliminary model and approach were initially introduced in our conference paper[28]. In this section, we provide a more comprehensive and self-contained presentation of our model and approach for completeness, which includes detailed problem formulation, improved algorithm with lower time complexity, performance analysis, and discussion on model limitation.

System model

We model the highway system as a directed graph $\mathcal{G} = (\mathcal{V}, \mathcal{E})$. The node set $\mathcal{V} = \mathcal{V}_r \cup \mathcal{V}_c$ consists of road connection points $\mathcal{V}_r$ and charging

stations $\mathcal{V}_c$. The edge set $\mathcal{E} \subset \mathcal{V} \times \mathcal{V}$ represents physical road segments. Each road segment $e \in \mathcal{E}$ has a length D_e and speed limits $[R_e^{lb}, R_e^{ub}]$, which define the minimum and maximum travel times $t_e^{lb} = D_e/R_e^{ub}$ and $t_e^{ub} = D_e/R_e^{lb}$, respectively. Without loss of generality, we assume homogeneous road conditions (e.g., grade) on each road segment. Following the model in refs. 5,28, we model the energy consumption rate (in kW) on segment e as a convex function of the traveling speed r_e, denoted $f_e(r_e) : [R_e^{lb}, R_e^{ub}] \to \mathbb{R}$. This function $f_e(r_e)$ is primarily determined by the road grade and the E-Truck's weight. Note that $f_e(r_e)$ can be negative on downhill segments due to regenerative braking[29]. Given the convexity of $f_e(\cdot)$, we can assume the E-Truck travels at a constant speed on segment e without loss of optimality [ref. 5, Lem. 1]. We ignore the acceleration and deceleration phases between road segments, since their contribution to overall time and energy consumption is typically negligible relative to the entire segment duration, as justified in refs. 5,28. The total energy consumed to traverse segment e in time t_e is then given by the perspective function $c_e(t_e) = t_e \cdot f_e(D_e/t_e)$, which is also convex in t_e by the convexity preserving property of the perspective function[30]. We assume $c_e(t_e)$ is nonincreasing in t_e, as the increasing domain can be excluded without loss of optimality[5,28].

At each charging station $v \in \mathcal{V}_c$, an E-Truck may wait for a time duration $t_w \in [t_w^{lb}, t_w^{ub}]$ and charge for a time duration $t_c \in [0, t_c^{ub}]$. The lower bound t_w^{lb} accounts for the minimum time required for a driver to stop and wait in a charging queue, etc. The upper bound t_w^{ub} is introduced to maintain model regularity and avoid excessively long waiting times. For ease of presentation, we employ a homogeneous lower bound across all charging stations and time periods while preserving the framework's broad applicability. Its extension to heterogeneous lower bounds for different charging stations is straightforward. A discussion on more sophisticated, dynamic waiting time estimation can be found in Discussion on Model Limitation.

We model the charging process at $v \in \mathcal{V}_c$ with a concave function $\Phi_v(t)$. It gives the battery SoC achieved after charging from an empty battery for a duration t. For an initial SoC β_v, the increase in SoC after charging for time t_c is given by:

$$\phi_v(t_c, \beta_v) = \Phi_v(\Phi_v^{-1}(\beta_v) + t_c) - \beta_v. \tag{2}$$

Here, Φ_v^{-1} denotes the inverse of the function Φ_v; see Supplementary Fig. 2 in Supplementary Information Section 5.1 for an illustration. While E-Trucks may support multiple charging modes, e.g., fast and regular charging, this work assumes the exclusive use of fast charging at all stations for simplicity. The inclusion of multiple charging schemes can be accommodated by modeling each scheme with a distinct charging node at the station and duplicating the adjacent road segments to connect these nodes. The concave charging function naturally captures the characteristic behavior of batteries, where the charging rate decreases as the state of charge (SoC) increases[29,31], and provides a more realistic modeling framework compared to the constant charging rate approximation[32].

At each charging station $v \in \mathcal{V}_c$, the carbon intensity is represented by a continuous function $\pi_v(\tau) : \mathbb{R} \to \mathbb{R}$ (in kg/kWh), where τ denotes the arrival time at node v. For simplicity, we set $\tau_0 = 0$ at the origin o. Note that carbon intensity data can be well predicted at hourly intervals, as discussed in ref. 33. Given this function, if an E-Truck with an initial SoC β_v begins charging at time τ_v and continues for a duration t_c, the resulting carbon footprint is expressed as:

$$F_v(\beta_v, t_c, \tau_v) = \frac{1}{\eta} \int_0^{t_c} \pi_v(\tau_v + \xi) \frac{\partial \phi_v}{\partial t}(\xi, \beta_v) d\xi. \tag{3}$$

Here, η (with $0 < \eta \le 1$) represents the battery's charging efficiency. The left partial derivative $\frac{\partial \phi_v}{\partial t}(\xi, \beta)$ corresponds to the charging rate at time ξ given initial SoC β. This carbon footprint function, which integrates the product of carbon intensity and instantaneous charging rate, yields a nonlinear and nonconvex expression.

A stage-expanded graph based problem formulation

We consider the problem of minimizing the carbon footprint for an E-Truck traveling from an origin $o \in \mathcal{V}$ to a destination $d \in \mathcal{V}$, under a hard deadline T and subject to the battery SoC constraints. The E-Truck begins with an initial SoC β_0 and has a battery capacity B, and is permitted to make up to N charging stops during the journey. Limiting the number of charging stops is reasonable in practice, as our analysis reveals that trips with 1500 miles typically only need 3–4 charging stops on average, while longer routes require proportionally more charging stops. Within our simulation dataset, the maximum observed charging requirement reached 12 stops for origin-destination pairs exceeding 3000 miles. This variable charging frequency reflects the realistic operational constraints of current E-truck technology and charging infrastructure, where trip distance directly influences charging strategy and route planning complexity.

In the following, we formulate the problem using the stage-expanded graph technique we mentioned in the "Results" section. A preliminary version of this formulation was presented in our conference paper[28]. Here, we provide a more comprehensive and self-contained presentation for completeness.

In the stage-expanded graph $\mathcal{G}_s$, a complete path is composed of $N+1$ subpaths that connect the origin, up to N charging stations, and the destination. The selection of the charging stop at each stage and the road segments used in each subpath are represented by the binary variables. Specifically, for every charging station $v \in \mathcal{V}_c$, a binary variable $y_v^i \in \{0,1\}$ is introduced, with $y_v^i = 1$ indicating that station v is chosen as the i-th charging stop. Similarly, for each subpath $i \in \{1, \ldots, N+1\}$ and each road segment $e \in \mathcal{E}$, a binary variable $x_e^i \in \{0,1\}$ is defined, where $x_e^i = 1$ denotes that segment e is selected in the i-th subpath. To simplify notation, we aggregate these variables as follows: $\mathbf{x}^i = \{x_e^i\}_{e \in \mathcal{E}}$, $\mathbf{x} = \{\mathbf{x}^i\}_{i=1}^{N+1}$, $\mathbf{y}^i = \{y_v^i\}_{v \in \mathcal{V}_c}$, and $\mathbf{y} = \{\mathbf{y}^i\}_{i=1}^{N+1}$. The feasible set for $(\boldsymbol{x}, \boldsymbol{y})$ is defined by the constraints that ensure connectivity, proper sequencing, and consistency across the subpaths and charging stops:

$$\mathcal{P} = \big\{(\mathbf{x}, \mathbf{y}) \,|\, x_e^i \in \{0,1\},\ \forall e \in \mathcal{E}, i \in \{1, \ldots, N+1\}, \tag{4a}$$

$$y_v^i \in \{0,1\}, \forall v \in \mathcal{V}_c, i \in \{0, \ldots, N+1\}, \tag{4b}$$

$$\sum_{e \in \mathrm{Out}(v)} x_e^i - \sum_{e \in \mathrm{In}(v)} x_e^i = y_v^{i-1} - y_v^i,\ \forall v \in \mathcal{V}_c, i \in \{1, \ldots, N+1\}, \tag{4c}$$

$$\sum_{v \in \mathcal{V}} y_v^i = 1,\ \sum_{v \in \mathcal{V}_c} y_v^i = 1,\ \forall i \in \{0, 1, \ldots, N+1\}, \tag{4d}$$

$$y_o^0 = 1, y_d^{N+1} = 1\big\}. \tag{4e}$$

In the above set, $\tilde{\mathcal{V}}_c = \mathcal{V}_c \cup \{o, d\}$. Out($v$) denotes the set of outgoing edges at node v and In(v) denotes the set of incoming edges at node v. The constraint (4c) enforces the flow conservation at each stage, ensuring that the path is continuous and connected. Constraint (4d) guarantees that exactly one charging station is selected per stage. Constraint (4e) specifies the boundary conditions at the origin o and the destination d. We also note that the feasible set $\mathcal{P}$ also accommodates paths with fewer than N charging stops, as the same charging station can be selected in consecutive stages.

Next, we introduce the decision variables for speed and charging planning. At each stage i and road segment e, we define t_e^i as the travel time on segment e during stage i. Additionally, for each charging station v considered as the i-th stop, we define $t_w^{i,v}$ and $t_c^{i,v}$ as the waiting time and charging time, respectively. These variables are

aggregated as follows: $\mathbf{t}^i = \{t_e^i\}_{e\in\mathcal{E}}$, $\mathbf{t}_w^i = \{t_w^{i,v}\}_{v\in\tilde{\mathcal{V}}_c}$, $\mathbf{t}_c^i = \{t_c^{i,v}\}_{v\in\tilde{\mathcal{V}}_c}$, and $\mathbf{t} = \{(\mathbf{t}^i, \mathbf{t}_w^i, \mathbf{t}_c^i)\}_{i=0}^{N+1}$. The corresponding feasible set is given by

$$\begin{aligned}\mathcal{T} \quad = \quad & \{\mathbf{t} \mid t_e^i \in [t_e^{lb}, t_e^{ub}], \forall e \in \mathcal{E}, i \in \{1, \ldots, N+1\}, \\ & t_w^{i,v} \in [t_w^{lb}, t_w^{ub}], t_c^{i,v} \in [0, t_c^{ub}], \forall v \in \tilde{\mathcal{V}}_c, i \in \{1, \ldots, N\}, \quad t_w^0 = t_c^0 = 0\}.\end{aligned} \tag{5}$$

We define τ_v^i as the arrival time at which the E-Truck arrives at charging station v for its i-th stop. These arrival times are collected into the vector $\boldsymbol{\tau} = \{\tau_v^i\}_{v\in\tilde{\mathcal{V}}_c, i\in\{0,\ldots,N+1\}}$. The feasible set for $\boldsymbol{\tau}$ is determined by constraints that ensure temporal consistency with the travel, waiting, and charging times:

$$\mathcal{T}_\tau = \{\boldsymbol{\tau} \mid \tau_v^i \in [0, T], \forall v \in \tilde{\mathcal{V}}_c, i \in \{0, \ldots, N+1\}\}. \tag{6}$$

We impose the constraint that the total duration for travel and charging during the i-th stage must fall within the predefined time window allocated for that stage:

$$\begin{aligned}\delta_i^\tau(\mathbf{x}, \mathbf{y}, \mathbf{t}, \boldsymbol{\tau}) = & \sum_{e\in\mathcal{E}} x_e^i t_e^i + \sum_{v\in\mathcal{V}_c} y_v^{i-1}(t_w^{i-1,v} + t_c^{i-1,v}) \\ & - \sum_{v\in\mathcal{V}_c}(y_v^i \tau_v^i - y_v^{i-1}\tau_v^{i-1}) \le 0.\end{aligned} \tag{7}$$

In the above constraint, the first term represents the travel time along the i-th subpath, while the second term accounts for the time spent at the $(i-1)$-th charging stop, including both waiting and charging. The third term corresponds to the total scheduled time duration allocated between the $(i-1)$-th and i-th charging stops, ensuring that the cumulative time used does not exceed the available window.

During the trip, it is crucial that our decisions prevent any battery overflow or underflow on each road segment, which may introduce numerous constraints and complicate the problem. Next, we seek to reduce the number of SoC constraints by leveraging a useful observation in practice.

We observe from empirical studies that regenerative braking provides only a limited amount of energy to the E-Truck, as noted in ref. 34. Given this practical insight, we demonstrate that by maintaining a mild reserve in the SoC upon arrival at a charging stop for a given stage, it is possible to ensure that the SoC remains positive throughout the entire subpath associated with that stage.

Specifically, let β_v^i represent the battery SoC of the E-Truck upon arrival at charging station v during the i-th stop. We aggregate these variables into the vector $\boldsymbol{\beta} = \{\beta_v^i\}_{v\in\tilde{\mathcal{V}}_c, i\in\{0,\ldots,N+1\}}$, whose feasible set is defined by:

$$\mathcal{S}_\alpha = \{\boldsymbol{\beta} \mid \beta_v^i \in [\alpha B, B], \forall v \in \tilde{\mathcal{V}}_c, i \in \{0, \ldots, N+1\}, \beta_o^0 = \beta_0\}, \tag{8}$$

where $\alpha \in [0, 1)$ is a parameter that sets a conservative lower bound on the SoC upon arrival at any charging station. The initial SoC at the origin is given by β_0. The SoC constraint that prevents battery depletion upon arrival at charging stop i is given by:

$$\begin{aligned}\delta_i^\beta(\mathbf{x}, \mathbf{y}, \mathbf{t}, \boldsymbol{\beta}) = & \sum_{e\in\mathcal{E}} x_e^i c_e(t_e^i) + \sum_{v\in\mathcal{V}_c} y_v^i \beta_v^i \\ & - \sum_{v\in\mathcal{V}_c} y_v^{i-1}\left(\beta_v^{i-1} + \phi_v(\beta_v^{i-1}, t_c^{i-1,v})\right) \le 0.\end{aligned} \tag{9}$$

In this expression, the first term corresponds to the total energy consumed along the i-th subpath, the second term represents the SoC upon arrival at the i-th charging stop, and the third term indicates the SoC after departing from the $(i-1)$-th charging stop. We then demonstrate that, under the condition that regenerative braking contributes only a minor amount of energy, a small value of α is adequate to maintain feasible SoC levels throughout each subpath.

Lemma 1. Consider an E-Truck traversing a subpath consisting of n road segments en route to a charging stop, starting with an initial SoC β_0. Let $c_i \in \mathbb{R}$ denote the energy consumed (or harvested, if negative) on the i-th segment. Provided the harvested energy from regenerative braking is relatively small such that:

$$\frac{1}{2}\sum_{i=1}^n (|c_i| - c_i) \le \frac{\alpha}{2(1-\alpha)}\sum_{i=1}^n c_i, \tag{10}$$

and if the initial SoC β_0 is large enough to support the cumulative energy consumption:

$$\beta_0 - \sum_{i=1}^n c_i \ge \alpha B, \tag{11}$$

then the E-Truck maintains a non-negative SoC throughout this subpath.

Note that the amount of energy harvested–represented by the left-hand side of inequality (10)–by an E-Truck traveling on the US highway network is indeed relatively small[34]. This is primarily because the maximum allowable grade on U.S. highways does not exceed 6%[35], which restricts the potential for large energy harvesting through regenerative braking. Our simulation results confirm that setting $\alpha = 0.06$ is adequate to maintain non-negative SoC in the majority of cases. Furthermore, a comparison with a lower bound scenario where $\alpha = 0$ reveals only a minor performance gap from introducing the conservative ratio α. The details of this comparison are provided in Supplementary Information Section 8.1. For scenarios involving non-negligible harvested energy, an extended treatment is provided in Supplementary Section 10.

The Carbon Footprint Optimization (CFO) problem is then formulated as follows:

$$CFO: \ \min F_0(\beta_d^{N+1}) + \sum_{i=1}^N \sum_{v\in\mathcal{V}_c} y_v^i F_v(\beta_v^i, t_c^{i,v}, \tau_v^i + t_w^{i,v}) \tag{12a}$$

$$\text{s.t. } \delta_i^\tau(\mathbf{x}, \mathbf{y}, \mathbf{t}, \boldsymbol{\tau}) \le 0, \ \forall i \in \{1, \ldots, N+1\}, \tag{12b}$$

$$\delta_i^\beta(\mathbf{x}, \mathbf{y}, \mathbf{t}, \boldsymbol{\beta}) \le 0, \ \forall i \in \{1, \ldots, N+1\}, \tag{12c}$$

$$\text{var.}(\mathbf{x}, \mathbf{y}) \in \mathcal{P}, \boldsymbol{\beta} \in \mathcal{S}_\alpha, \boldsymbol{\tau} \in \mathcal{T}_\tau, \mathbf{t} \in \mathcal{T}. \tag{12d}$$

Our objective is to minimize the carbon footprint (12a), where $F_0(\beta_d) = \pi_0 \cdot (\beta_0 - \beta_d)_+ = \pi_0 \cdot \max\{0, \beta_0 - \beta_d\}$ represents the carbon footprint for the used electricity in the initial battery and π_0 is the carbon intensity of the electricity in the initial battery. Constraint (12b) is the time scheduling constraint at each stage, the details of which are referred to (7). Constraint (12c) is the SoC constraint for each subpath, the details of which could be referred to (9).

The following theorem presents the hardness result of the CFO problem.

Theorem 1. The CFO problem is NP-hard. Further, it is NP-hard even just to find a feasible solution for the problem.

This hardness result was initially presented in our conference paper[36] without the proof. Here we provide a proof in Supplementary Section 11.2 for completeness. Theorem 1 implies that unless P = NP, there is no polynomial-time algorithm that can generate a feasible solution to some CFO problem. Such a result indicates that finding a feasible solution efficiently is difficult in the worst case. However, we observe that the hard case only happens when the deadline is stringent. In particular, we

consider the following problem, which seeks to find the fastest solution subject to the SoC feasibility constraints:

$$T_f = \min \sum_{i=1}^{N} \sum_{v \in \mathcal{V}_c} y_v^i (t_c^{i,v} + t_w^{i,v}) + \sum_{i=1}^{N+1} \sum_{e \in \mathcal{E}} x_e^i t_e^i \tag{13a}$$

$$\text{s.t. } \delta_i^{\beta}(\mathbf{x}, \mathbf{y}, \mathbf{t}, \boldsymbol{\beta}) \le 0, \ \forall i \in \{1, \ldots, N+1\} \tag{13b}$$

$$\text{var. } (\mathbf{x}, \mathbf{y}) \in \mathcal{P}, \boldsymbol{\beta} \in \mathcal{S}_{\alpha}, \mathbf{t} \in \mathcal{T}. \tag{13c}$$

We denote the optimal solution of (13) as T_f. Note that when the user-specified deadline T in the CFO problem (12) is the same as the minimum time T_f, it becomes difficult to find a feasible solution of (12) because the problem (13) is NP-hard and finding a feasible solution to the CFO problem (12) is as difficult as finding the optimal solution to the fastest solution for (13). In practice, however, the deadline T is usually determined by the customer and may not be close to the minimum possible travel time T_f. In the following, we shall assume that the deadline T is larger than the total time of a practical baseline solution, and our approach starts with a feasible solution produced by such a practical baseline. We also provide a discussion on how to handle the case when such an assumption fails and the deadline $T = (1+\epsilon)T_f$ is close to T_f in Supplementary Section 10.

An efficient algorithm with performance guarantees

In this section, we introduce an efficient dual-based algorithm for the CFO problem, leveraging structural properties derived from the formulation in (12). The algorithm utlizes a partially dualization technique[5,6,37] for the constraints (12b) and (12c). After the partial dualization, we can convert the original problem (12) into a tractable dual problem that can be decomposed into small subproblems and a shortest path problem on the stage-expanded graph. We then update the dual variables by the subgradient method to obtain the final solution. Note that a preliminary version of this algorithm was presented in our conference paper[28]. In this extended work, we offer a more detailed elaboration of the algorithm, accompanied by a methodological improvement that enhance its clarity and reduce its computational complexity.

To construct a partially-relaxed dual formulation of the CFO problem presented in (12), we relax constraints (12b) and (12c), associating dual variables λ_i^{τ} and λ_i^{β} with each, respectively. The dual variable λ_i^{τ} represents the price of the scheduled deadline at the stage i, and λ_i^{β} represents the price of the SoC at the stage i. The Lagrangian function is given by combining the objective function and constraints using dual variables, i.e.,

$$L(\mathbf{x}, \mathbf{y}, \mathbf{t}, \boldsymbol{\beta}, \boldsymbol{\tau}, \boldsymbol{\lambda}) = F_0(\beta_d^{N+1}) + \sum_{i=1}^{N} \sum_{v \in \mathcal{V}_c} y_v^i F_v(\beta_v^i, t_c^{i,v}, \tau_v^i + t_w^{i,v}) \tag{14a}$$

$$+ \sum_{i=1}^{N+1} \lambda_i^{\tau} \delta_i^{\tau}(\mathbf{x}, \mathbf{y}, \mathbf{t}, \boldsymbol{\tau}) + \sum_{i=1}^{N+1} \lambda_i^{\beta} \delta_i^{\beta}(\mathbf{x}, \mathbf{y}, \mathbf{t}, \boldsymbol{\beta}). \tag{14b}$$

Here we stack the dual variables into a vector $\boldsymbol{\lambda} = (\boldsymbol{\lambda}^{\beta}, \boldsymbol{\lambda}^{\tau})$. The definition of each term in the above Lagrangian function could be found in the CFO problem in (12).

The corresponding dual problem then seeks to maximize the dual function $D(\boldsymbol{\lambda})$, which is the minimum value of the Lagrangian function $L(\cdot)$ given a $\boldsymbol{\lambda}$, i.e.,

$$D(\boldsymbol{\lambda}) = \min_{\substack{(\mathbf{x}, \mathbf{y}) \in \mathcal{P}, \\ \boldsymbol{\beta} \in \mathcal{S}_{\alpha}, \boldsymbol{\tau} \in \mathcal{T}_{\tau}, \mathbf{t} \in \mathcal{T}}} L(\mathbf{x}, \mathbf{y}, \mathbf{t}, \boldsymbol{\beta}, \boldsymbol{\tau}, \boldsymbol{\lambda}). \tag{15}$$

The dual problem is then given by

$$\max_{\boldsymbol{\lambda} \ge 0} D(\boldsymbol{\lambda}). \tag{16}$$

In the dual subgradient algorithm used to solve the problem, efficient computation of the dual function $D(\boldsymbol{\lambda})$ is crucial. Here, we proceed to discuss the methodology for computing $D(\boldsymbol{\lambda})$ efficiently. After plugging in the definitions and rearranging the terms in (15), we observe that computing $D(\boldsymbol{\lambda})$ given $\boldsymbol{\lambda}$ is to solve a two-level optimization problem. The inner level involves multiple independent subproblems, each corresponding to an individual road segment or a charging station. The outer level involves a combinatorial optimization problem focusing on path and charging station selection.

$$D(\boldsymbol{\lambda}) = D_1(\boldsymbol{\lambda}) + \min_{\beta_d^{N+1} \in [\alpha B, B]} \left(\lambda_{N+1}^{\beta} \beta_d^{N+1} + F_0(\beta_d^{N+1}) \right) \tag{17a}$$

$$+ \min_{(\mathbf{x}, \mathbf{y}) \in \mathcal{P}} \Bigg(\sum_{i=1}^{N+1} \sum_{e \in \mathcal{E}} x_e^i \underbrace{\min_{t_e^i \in [t_e^{lb}, t_e^{ub}]} g_e^i(\boldsymbol{\lambda}, t_e^i)}_{w_e^i(\boldsymbol{\lambda}):\text{speed planning}} \tag{17b}$$

$$+ \sum_{i=1}^{N} \sum_{v \in \mathcal{V}_c} y_v^i \underbrace{\min_{\substack{t_c^{i,v} \in [0, t_c^{ub}], t_w^{i,v} \in [t_w^{lb}, t_w^{ub}], \\ \beta_v^i \in [\alpha B, B], \tau_v^i \in [0, T]}} h_v^i(\boldsymbol{\lambda}, t_c^{i,v}, t_w^{i,v}, \beta_v^i, \tau_v^i)}_{\sigma_v^i(\boldsymbol{\lambda}):\text{charging planning}} \Bigg), \tag{17c}$$

where $D_1(\boldsymbol{\lambda}) = -\lambda_{N+1}^{\tau} T - \beta_0 \lambda_1^{\beta}$ is a constant for any given $\boldsymbol{\lambda}$ and the functions $g_e^i(\cdot)$ and $h_v^i(\cdot)$ are auxiliary functions for ease of presentation. In particular, the function $g_e^i(\boldsymbol{\lambda}, t_e^i)$ is given by

$$g_e^i(\boldsymbol{\lambda}, t_e^i) = \lambda_i^{\tau} t_e^i + \lambda_i^{\beta} c^e(t_e^i), \tag{18}$$

and the function $h_v^i(\boldsymbol{\lambda}, t_c^{i,v}, t_w^{i,v}, \beta_v^i, \tau_v^i)$ is given by

$$\begin{aligned} h_v^i\left(\boldsymbol{\lambda}, t_c^{i,v}, t_w^{i,v}, \beta_v^i, \tau_v^i\right) &= F_v\left(\beta_v^i, t_c^{i,v}, \tau_v^i + t_w^{i,v}\right) + \lambda_{i+1}^{\tau}\left(t_w^{i,v} + t_c^{i,v}\right) \\ &+ \left(\lambda_{i+1}^{\tau} - \lambda_i^{\tau}\right)\tau_v^i + \left(\lambda_i^{\beta} - \lambda_{i+1}^{\beta}\right)\beta_v^i - \lambda_{i+1}^{\beta}\phi_v\left(\beta_v^i, t_c^{i,v}\right). \end{aligned} \tag{19}$$

Intuitively, $g_e^i(\boldsymbol{\lambda}, t_e^i)$ includes all terms associated with the road segment e in stage i, representing the cost of traveling time t_e^i under the dual prices $\boldsymbol{\lambda}$. $h_v^i(\boldsymbol{\lambda}, t_c^{i,v}, t_w^{i,v}, \beta_v^i, \tau_v^i)$ includes all terms associated with charging station v at stage i, representing the cost of arriving at time τ_v^i with SoC β_v^i, waiting $t_w^{i,v}$, and charging for $t_c^{i,v}$ time under the dual prices $\boldsymbol{\lambda}$.

Next, we show how to efficiently compute the dual function $D(\boldsymbol{\lambda})$ based on (17), which includes solving the three types of subproblems (17a), (17b) and (17c) and determining the path and charging station selection $(\mathbf{x}, \mathbf{y}) \in \mathcal{P}$.

The first type of subproblem in (17a) is a single-variable optimization problem with respect to β_d^{N+1}, which can be solved efficiently. We define its optimal value as

$$\rho(\boldsymbol{\lambda}) = \min_{\beta_d^{N+1} \in [\alpha B, B]} \left(\lambda_{N+1}^{\beta} \beta_d^{N+1} + F_0\left(\beta_d^{N+1}\right) \right). \tag{20}$$

The second type of subproblem in (17b) is a single-variable optimization problem with respect to t_e^i. We define its optimal value as

$$w_e^i(\boldsymbol{\lambda}) = \min_{t_e^i \in [t_e^{lb}, t_e^{ub}]} g_e^i(\boldsymbol{\lambda}, t_e^i), \tag{21}$$

where the function $g_e^i(\cdot)$ is defined in (18). Given any $\boldsymbol{\lambda}$, the above problem is a single-variable optimization problem for every edge e at stage i, which can be solved efficiently. The above optimization problem aims to find the optimal travel time t_e^i for each edge e at stage i that balances the trade-off between the traveling time t_e^i and the energy consumption $c_e(t_e)$ with the weighting factor $\boldsymbol{\lambda}$.

The third type of subproblem in (17c) is a 4-variable optimization problem with respect to $t_c^{i,v}, t_w^{i,v}, \beta_v^i$ and τ_v^i. We define its optimal value as

$$\sigma_v^i(\boldsymbol{\lambda}) = \min_{\substack{t_c^{i,v} \in [0, t_c^{ub}], t_w^{i,v} \in [t_w^{lb}, t_w^{ub}], \\ \beta_v^i \in [\alpha B, B], \tau_v^i \in [0, T]}} h_v^i(\boldsymbol{\lambda}, t_c^{i,v}, t_w^{i,v}, \beta_v^i, \tau_v^i). \tag{22}$$

Given the dual variable $\boldsymbol{\lambda}$ that gives the tradeoff between the objective and the constraints, the above optimization problem aims to find the optimal charging time $t_c^{i,v}$, waiting time $t_w^{i,v}$, battery SoC β_v^i and the arriving time τ_v^i at stage i for each charging station v. The value of $\sigma(\boldsymbol{\lambda})$ can be computed in $O(M^4/\epsilon_1^4)$ time using a Branch and Bound (BnB) approach[38], which involves sovling the fixed-size, 4-variable nonconvex problem in (22). Here, $M = \max\{t_c^{ub}, t_w^{ub}, B, T\}$ represents the diameter of the box constraint in subproblem (22), and ϵ_1 denotes the desired solution accuracy.

Upon resolving the above inner level subproblems (20), (21) and (22), we can rewrite the dual function $D(\boldsymbol{\lambda})$ in (17) in terms of ρ, w, σ as follows:

$$D(\boldsymbol{\lambda}) = D_1(\boldsymbol{\lambda}) + \rho(\boldsymbol{\lambda}) + \min_{(\mathbf{x},\mathbf{y}) \in \mathcal{P}} \left(\sum_{i=1}^{N+1} \sum_{e \in \mathcal{E}} w_e^i(\boldsymbol{\lambda}) x_e^i + \sum_{i=1}^{N} \sum_{v \in \mathcal{V}_c} \sigma_v^i(\boldsymbol{\lambda}) y_v^i \right). \tag{23}$$

While the outer-level problem in (23) initially presents itself as a complex integer program, it can be effectively transformed into a shortest path problem on the stage-expanded graph $\mathcal{G}_s$. Here, each edge e at stage i is assigned a weight $w_e^i(\boldsymbol{\lambda})$, and virtual edges linking node v from stage i to $i+1$ are given weights σ_v^i. This reformulation not only simplifies the problem but also leads to a improvement in computational complexity (cf. Proposition 1) compared to our prior work[28], which relied on a more intricate graph construction.

Given any dual variable $\boldsymbol{\lambda}$, the value of $D(\boldsymbol{\lambda})$ can be efficiently computed by first solving subproblems (20), (21), and (22), and subsequently addressing the outer problem (23) using shortest-path algorithms on the stage-expanded graph. To iteratively refine the dual variable $\boldsymbol{\lambda}$, we employ a dual subgradient method. Let $\boldsymbol{\lambda}[k]$ represent the dual variable at iteration k. The update rule is applied as follows:

$$\lambda_i^\beta[k+1] = \left(\lambda_i^\beta[k] + \theta_k \underbrace{\delta_i^\beta\left(\mathbf{x}^*[k], \mathbf{y}^*[k], \mathbf{t}^*[k], \boldsymbol{\beta}^*[k]\right)}_{\delta_i^\beta[k]} \right)_+, \tag{24a}$$

$$\lambda_i^\tau[k+1] = \left(\lambda_i^\tau[k] + \theta_k \underbrace{\delta_i^\tau\left(\mathbf{x}^*[k], \mathbf{y}^*[k], \mathbf{t}^*[k], \boldsymbol{\tau}^*[k]\right)}_{\delta_i^\tau[k]} \right)_+. \tag{24b}$$

The values $\mathbf{x}^*[k]$, $\mathbf{y}^*[k]$, $\mathbf{t}^*[k]$, $\boldsymbol{\beta}^*[k]$, $\boldsymbol{\tau}^*[k]$ are obtained by solving subproblems (23), (21), and (22) using the current dual variable $\boldsymbol{\lambda}[k]$. These solutions yield the subgradient components $\delta_i^\beta[k]$ and $\delta_i^\tau[k]$ for $D(\boldsymbol{\lambda})$. We use the operator $(a)_+$ to represent $\max\{0, a\}$, and θ_k denotes the adaptive step size at iteration k.

The overall approach is outlined in Box 1. We first initialize the solution by the baseline solution $\mathbf{sol}_0$ (cf. discussion below Theorem 1) and then iteratively compute $D(\boldsymbol{\lambda})$ and update $\boldsymbol{\lambda}$ via the subgradient direction. Intuitively, the dual variables $\boldsymbol{\lambda}$ can be viewed as penalties associated with violating the scheduled deadline and the battery SoC constraints. A higher value of λ_i^β, for example, places larger emphasis on the constraint δ_i^β, leading to several consequences. First, it increases the influence of energy cost in (18), which in turn leads to longer travel times solved from the edge subproblem (21). Meanwhile, an increase in λ_i^β leads to a decrease in the scheduled battery SoC β_v^i at the i-th stop, while simultaneously increasing β_v^{i-1} and extending the charging time $t_c^{i,v}$ at the $(i-1)$-th stop. This indicates that a higher λ_i^β amplifies the difference in scheduled SoC between consecutive charging stops $(i-1)$ and i. A similar interpretation holds for the dual variable λ_i^τ. Essentially, the algorithm in Box 1 aims to iteratively update the dual variables to identify a solution that balances the objective and the penalties from the constraints.

We now present a theoretical analysis of our approach, establishing three key properties: (i) the algorithm guarantees convergence with a rate of $O(1/\sqrt{K})$, with K number of iterations; (ii) the computational complexity per iteration remains polynomial with respect to the graph size; and (iii) under certain conditions, the algorithm will produce the optimal solution, while otherwise will produce the solution with bounded suboptimality. The proofs are available in the Supplementary Information.

Consistent with classical subgradient methods[39], the proposed algorithm in Box 1 achieves convergence to the dual optimal value at the same $O(1/\sqrt{K})$ rate.

BOX 1

A Dual Subgradient Algorithm for CFO

Initialization:
Set the initial solution $\mathbf{sol} \leftarrow \mathbf{sol}_0$.
Set the initial dual variables: $\boldsymbol{\lambda}[1] \leftarrow 0$.

Main algorithm:
for $k \leftarrow 1$ to K **do**
  Solve the dual problem (15) and compute $\mathbf{sol}^+$ with $\boldsymbol{\lambda}[k]$:

$$D(\boldsymbol{\lambda}) = \min_{\substack{(\mathbf{x},\mathbf{y}) \in \mathcal{P}, \\ \boldsymbol{\beta} \in \mathcal{S}_\alpha, \boldsymbol{\tau} \in \mathcal{T}_\tau, \mathbf{t} \in \mathcal{T}}} L(\mathbf{x}, \mathbf{y}, \mathbf{t}, \boldsymbol{\beta}, \boldsymbol{\tau}, \boldsymbol{\lambda}).$$

  if $\delta_i^\beta[k] = 0$ and $\delta_i^\tau[k] = 0, \forall i \in \{1, \ldots, N+1\}$ **then**
    return sol $\leftarrow \mathbf{sol}^+$
  end if
  if $\delta_i^\beta[k] \le 0$ and $\delta_i^\tau[k] \le 0, \forall i \in \{1, \ldots, N+1\}$
    and $\mathbf{sol}^+$ iccurs less carbon footprint objective **then**
    Update the solution $\mathbf{sol} \leftarrow \mathbf{sol}^+$
  end if
  Compute $\boldsymbol{\lambda}[k+1]$ via the dual subgradient direction (24):

$$\lambda_i^\beta[k+1] = \left(\lambda_i^\beta[k] + \theta_k \delta_i^\beta[k]\right)_+,$$
$$\lambda_i^\tau[k+1] = \left(\lambda_i^\tau[k] + \theta_k \delta_i^\tau[k]\right)_+.$$

end for
return sol

Theorem 2. Let D^* denote the optimal dual objective, and $\overline{D}_K$ represent the maximum dual value achieved over K iterations of the algorithm in Box 1. Using a constant step size $\theta_k = \frac{1}{\sqrt{K}}$ for all $1 \le k \le K$, there exists a positive constant C such that the following holds:

$$D^* - \overline{D}_K \le \frac{C}{\sqrt{K}}. \tag{25}$$

Theorem 2 shows that a constant step size $1/\sqrt{K}$ is sufficient to achieve a convergence rate of $O(1/\sqrt{K})$. To obtain faster convergence, one may adaptively update the step sizes[40] or modify the subgradient directions[41].

Next, we provide a summary of the time complexity per iteration for the algorithm outlined in Box 1, as described in the following proposition.

Proposition 1. The time complexity per iteration of the algorithm in Box 1 is given by

$$O\left((N+1)^2|\mathcal{V}||\mathcal{E}| + N|\mathcal{V}_c|\frac{M^4}{\epsilon_1^4}\right), \tag{26}$$

where $M = \{t_c^{ub}, t_w^{ub}, B, T\}$ and ϵ_1 denotes the tolerance level used to determine convergence when solving the subproblems (22).

Proposition 1 establishes that, the computational complexity per iteration of our approach remains bounded by a polynomial function of the graph size. Note that as compared to our conference version[28], the time complexity per iteration has been improved by a factor of $|\mathcal{V}_c|$, mainly due to a more efficient treatment for solving the outer integer problem (23).

Recall that Theorem 2 ensures that the algorithm in Box 1 converges to a solution in $O(1/\epsilon_0^2)$ number of iterations, with the accuracy tolerance ϵ_0. By combining Proposition 1 and Theorem 2, the total time complexity of the algorithm in Box 1 is given by

$$O\left(\frac{1}{\epsilon_0^2}\left((N+1)^2|\mathcal{V}||\mathcal{E}| + N|\mathcal{V}_c|\frac{M^4}{\epsilon_1^4}\right)\right). \tag{27}$$

Note that a convergence to the dual optimum does not necessarily guarantee convergence to the primal optimum due to the potential existence of a duality gap. We thus establish the following posterior bound on the suboptimality.

Theorem 3. Let OPT denote the optimal objective value for the problem in (12). If the algorithm described in Box 1 generates a feasible solution during iteration $k \ge 1$ with an objective value of ALG, then the optimality gap can be bounded as follows:

$$ALG - OPT \le -\sum_{i=1}^{N+1}\left(\lambda_i^{\beta}[k]\delta_i^{\beta}[k] + \lambda_i^{\tau}[k]\delta_i^{\tau}[k]\right). \tag{28}$$

Note that this posterior bound in (28) can be evaluated during each iteration of the algorithm in Box 1, enabling early termination when a desired accuracy level is reached. Furthermore, Theorem 3 also establishes an optimality condition for the generated solution, as formalized in the following corollary.

Corollary 1. If the algorithm in Box 1 returns a feasible solution in line 9, then the solution is optimal.

Discussion on model limitation

While our model and approach provide a comprehensive framework that captures the essential components of carbon-optimized E-Truck operations, there are several real-world considerations that are not explicitly modeled in this study. Below, we analyze how these considerations impact carbon footprint optimization for E-trucks and discuss potential integration approaches within our methodology.

Driver work/rest regulations. Regulatory frameworks worldwide mandate specific driver work and rest periods to ensure safety and well-being. In the United States, Federal Motor Carrier Safety Administration (FMCSA) Hours of Service (HOS) rules require: (i) maximum 11 h driving within a 14-h workday followed by 10 consecutive hours rest, (ii) mandatory 30-min break after 8 h driving, and (iii) weekly limits of 60 h over 7 days or 70 h over 8 days. Similarly, EU Drivers' Hours Rules mandate (i) a maximum of 9 h daily driving, (ii) a 45-min break after 4.5 h driving, and (iii) a 45-h weekly rest period. While existing literature addresses driver scheduling under work/rest regulations[42,43], these studies neither consider E-truck routing with intermittent charging requirements nor time-dependent carbon intensity dynamics, limiting their direct applicability to our problem. Given that deliveries in our scenarios may require 15–60 h of driving, the most relevant constraints are short breaks and mandatory rest periods. These requirements alter arrival times at charging stations, thereby affecting the carbon intensity of charging energy. Our framework could accommodate these regulations by synchronizing rest stops with charging schedules and incorporating mandatory breaks into route stages. Take the US HOS rules as an example, we could implement the following adaptations: (i) We can group every two stages and add a constraint that the total driving time in these two stages should not exceed 11 h. We can then add a constraint that the minimum waiting time t_w^{lb} after the second stage in the group should be 10 h. (ii) We can add a constraint that the total driving time in every stage should not exceed 8 h, and the minimum waiting time t_w^{lb} after every stage should be 30 min. The choice of t_w^{lb} and the number of stages in a group can be adjusted based on the specific regulations and operational requirements. Our proposed scheme can be readily extended without new difficulty to solve the problem with these new constraints by following the same mathematical derivation steps in the "Methods" section. This adaptation would maintain regulatory compliance while leveraging dynamic carbon intensity variations across different charging times and locations. However, it may incur optimality loss as it reduces the feasible solution space. A comprehensive evaluation of work/rest regulation impacts on carbon savings merits dedicated future investigation.

Payload restrictions. Payload constraints encompass two dimensions: (i) vehicle-specific maximum load capacity and (ii) road-specific axle load limits. Regarding vehicle capacity, our current framework assumes a predetermined payload based on transportation requirements, with appropriate truck selection occurring prior to route optimization. Since payload directly influences energy consumption[44], incorporating diverse truck types and payload configurations would enhance assessment precision. Our approach can be extended to broader vehicle and payload scenarios, which should be straightforward. For road-specific restrictions, we can preprocess the transportation network by removing edges where the payload exceeds allowable limits, ensuring regulatory compliance. Our approach then operates on this filtered network without requiring framework modifications. We also note that stricter payload regulations effectively reduce the feasible solution space, potentially limiting achievable carbon savings.

Weather impacts. Weather conditions affect three key model components: (i) carbon intensity function $\pi_v(\tau)$ through wind and solar irradiance variations, (ii) energy consumption function $c_e(t_e)$ via wind speed and temperature effects, and (iii) travel speed limits during adverse conditions. For carbon intensity, state-of-the-art prediction tools like CarbonCast[45] already incorporate weather impacts on renewable energy generation and grid carbon intensity[33,45]. Our framework implicitly accounts for weather-related carbon intensity

variations through these prediction systems. For energy consumption and speed limits, we can integrate weather forecasts as additional model parameters[46] to enhance realism and accuracy. Implementation would involve incorporating weather predictions to update these functions, then applying our approach with modified inputs. To address prediction uncertainties and unexpected conditions, we could incorporate buffers in travel deadlines and battery capacity while enabling dynamic re-planning when conditions change drastically.

Dynamic speed limits. Dynamic speed limits due to time-varying traffic conditions or heterogeneous road types could impact the design space of carbon-optimized operation. Integrating dynamic speed limits into the model would require real-time updates to travel speeds and route plans, potentially leveraging traffic condition predictions. Our stage-expanded graph approach could be adapted to accommodate these dynamic travel speed limits. For example, we can divide the time into different traffic phases (e.g., morning and evening rush hours)[47] and treat each traffic phase as another type of stage. Therefore, in the stage-expanded graph, each stage also corresponds to a traffic phase, and our approach can thus be adapted to accommodate the dynamic travel speed limits. Such adaptation, however, may complicate the model and thus requires further investigation.

Sophisticated queueing model for charging stations. Recall that for ease of presentation, we employ a homogeneous lower bound of the waiting time t_w^{lb} across all charging stations and time periods while preserving the framework's broad applicability. Its extension to heterogeneous lower bounds for different charging stations is straightforward. More sophisticated, dynamic waiting time estimation could incorporate queuing theory approaches based on charging station capacity and traffic-derived arrival rates[48,49], or simulation-based methodologies[50]. These refined queuing estimates could subsequently be integrated into our optimization framework for enhanced delivery planning accuracy.

We would like to note that, while more sophisticated models would undoubtedly increase realism, our work represents a comprehensive framework addressing carbon footprint optimization in E-truck operations. Our primary objective is to demonstrate the potential of carbon-aware E-truck strategies within broader decarbonization initiatives. We believe our current modeling approach provides a robust foundation for establishing this potential, while more sophisticated models constitute valuable directions for future research.

Simulation setup

Transportation network. We utilize the U.S. highway network data from the Map-based Educational Tools for Algorithm Learning (METAL) project[51]. The constructed network comprises 84,504 nodes and 178,238 edges. Road segment grades are calculated using elevation data from the Shuttle Radar Topography Mission (SRTM)[52], based on the endpoints of each segment. For real-time traffic conditions, we integrate the speed data obtained from HERE Maps[20].

Energy consumption model. To obtain energy consumption data, we employ the FASTSim simulator[53], and evaluate the energy consumption across varying driving speeds (ranging from 10 mph to 70 mph in increments of 0.2 mph) and road grades (from −6 to 6% in steps of 0.25%). It is worth noting that the maximum permissible grade for interstate highways in the United States, as specified in ref. 35, is a 6-m elevation change over 100 meters of road length. We subsequently fit the collected energy consumption data using cubic polynomial functions, which are also used in prior studies[5,37,47]. Among heavy-duty E-Truck models, we select the Tesla Semi[54] as our primary vehicle model based on several key considerations specific to our U.S.-focused case study. The Tesla Semi currently offers the longest commercially advertised range (500 miles) among heavy-duty electric trucks available in the U.S. market. While alternative electric truck models are emerging, their typical operational ranges of 200–300 miles are not well-suited for the long-haul transportation scenarios examined in this study. More importantly, the Tesla Semi's 500-mile range represents what we believe to be a realistic and achievable benchmark for electric truck capabilities as the technology matures and becomes more widely adopted. This range specification allows us to model scenarios that reflect the anticipated operational potential of electric trucking rather than being constrained by current technological limitations. For comparative reference, we have included a comprehensive overview of available electric truck models in the U.S. market in Table 2. We set the battery capacity to $B = 1000$ kWh (derived from manufacturer-reported energy consumption rates) and the gross vehicle weight to 36 tons, consistent with class 8 truck standards for highway freight.

Origin destination pair and start time. We collect origin-destination pairs from the Freight Analysis Framework (FAF)[13]. We divide the long-haul origin-destination pairs into the following four distance categories: 500–1000 miles, 1000–1500 miles, 1500–2000 miles, and 2000+ miles. We select the top 100 pairs based on freight values from each group, resulting in a total of 400 origin-destination pairs. For each origin-destination pair, we select the corresponding nearest nodes in the highway network graph as the origin and destination nodes, respectively. For each origin-destination pair, we conduct the simulation with the start time of travel at 8:00 AM on February 1st, May 1st, August 1st, and November 1st, 2024, to account for seasonal variations in carbon intensity. For future projections, we use the same date and time with varying years.

Charging station data. Given the limited availability of dedicated truck-specific charging networks, we collect the location data of light-duty EV charging stations from OpenStreetMap (OSM)[19]. While these stations primarily serve light-duty EVs, we consider them operationally relevant for heavy-duty electric truck analysis for two critical reasons. First, dedicated truck-specific charging networks remain limited in current U.S. infrastructure deployment, making existing charging locations the most realistic foundation for near-term planning. Second, existing light-duty EV charging infrastructure can be technically adapted to accommodate heavy-duty electric trucks through power scaling and connector modifications, as demonstrated in recent infrastructure studies[55]. Consequently, OSM's charging location data provides a realistic and practical foundation for heavy-duty electric truck infrastructure planning and operational optimization studies within the U.S. context. We merge the charging stations with the same locations into a single charging station. The dataset includes 1, 636 charging stations, and we model their charging functions using a piecewise linear approximation with breakpoints at 0%, 80%, 85%, 90%, 95%, and 100% battery SoC[29]. This model indicates that the studied E-Truck can be charged from 0% to 80% in 48 min. A visual representation of this charging process is provided in Supplementary Fig. 2 within Supplementary Information Section 5.1. For carbon intensity data, we utilize the Cambium datasets[15], from which we derive a

Table 2 | A summary of the available heavy-duty E-Truck models in the US

Model	Range	Charging Time
Kenworth T680E	150 mile	125 min (80%)
Peterbilt 579EV	150 mile	120 min (90%)
Freightliner eCascadia	150–230 mile	90 min (80%)
Volvo VNR Electric	275 mile	90 min (80%)
Nikola Tre BEV	330 mile	160 min (80%)
Tesla Semi	500 mile	40 min (80%)

piecewise linear carbon intensity function $\pi(\cdot)$ for each charging station. The charging efficiency η is set to 0.9[56].

ICE truck model. We adopt the parameters of the Kenworth T800 trailer[57] for the ICE truck model. We set the same total weight of 36 tons as the E-Truck model. The FASTSim simulator is then employed to gather fuel consumption data for the ICE trucks, from which we derive the corresponding energy consumption function. To quantify carbon emissions, we apply the CO_2 emission factor for diesel provided by the EIA[58]. According to the data, a diesel-powered ICE truck emits 10.19 kg of CO_2 per gallon of diesel consumed, which is equivalent to 0.25 kg of CO_2 per kWh of energy. We assume that the ICE trucks begin its journey with a full fuel tank at the origin. Given the ubiquitous refueling infrastructure for conventional vehicles, we further assume that ICE trucks can access refueling stations with negligible detour or delay during transit.

Carbon-efficient operations for ICE trucks and hydrogen FCE-trucks. For ICE trucks, the carbon-efficient operation is equivalent to the energy-efficient operation, as we assume ICE trucks' refueling takes negligible time along the transportation task. The CFO problem reduces the energy-efficient driving problem for ICE trucks, and our approach reduces to the dual-based method in[5]. We thus use the algorithm in[5] to compute the carbon-optimized operation for ICE trucks. For hydrogen FCE-Trucks, we use the same energy consumption model as E-Trucks. We assume all the hydrogen fuel consumed by FCE-Trucks is produced by electrolysis of water using the electricity from the same region as the hydrogen refueling station[59]. Additionally, we assume that the hydrogen refueling stations are co-located with the electric charging stations. Because the FCE-Truck usually has a longer range and a shorter refueling time than the E-Truck, a feasible E-Truck operation is also a feasible hydrogen FCEV truck operation for the same transportation task. In the simulation, we adopt the same carbon-optimized operation for E-Trucks to the hydrogen FCE-Trucks. We then evaluate the carbon footprint of FCE-Trucks with an electrolysis efficiency of 80%[60] and a hydrogen-to-electricity efficiency of 60%[61]. Although this direct application is sub-optimal, it still results in a substantial reduction in carbon emissions for FCE-Trucks. With our primary focus on E-Trucks, we defer a more comprehensive study on the carbon-optimized operation for FCE-Trucks to future research.

Electric grid projection. We use the electric grid projection data from the Cambium dataset[15]. We use the following three scenarios: (i) BAU: the business-as-usual scenario, called "Mid-case" in the Cambium dataset; (ii) CONSERVATIVE: a conservative projection that assumes the cost of renewable investment remains high in the future, called "High Renewable Energy and Battery Costs" in the Cambium dataset; (iii) OPTIMISTIC: an optimistic projection that achieves the electric grid meets the full decarbonization target by 2035[16], called "Mid-case with 100% Decarbonization by 2035" in the Cambium dataset. By default, we use carbon intensity data in 2024 with the BAU scenario.

Vehicle adoption projection. We use the vehicle adoption projection data from ref. 14. We select the data for long-haul heavy-duty trucks (class 7–8). We do not differentiate the hybrid electric trucks and ICE trucks in the simulation as they are both powered by diesel, and hybrid electric trucks contribute little fuel efficiency improvement in the long-haul task[61]. We use the following three different scenarios for the vehicle adoption projection: (i) NORMAL: the scenario with central assumption, called "Central" in ref. 14; (ii) ADVANCED: the scenario with lower charging infrastructure cost and higher utilization, called "Adv. Electricity" in ref. 14. (iii) CONSTRAINED: the scenario with constrained FCE-Truck and E-Truck technology advancement, called "Cons. ZEV Tech Progress" in ref. 14.

Baseline comparison. We evaluate and compare the following truck operation strategies: (i) CARBON: our proposed approach focused on minimizing carbon footprint; (ii) ENERGY: a variant of our approach where the objective is to minimize energy consumption, achieved by setting a uniform carbon intensity $\pi(\cdot) \equiv 1$; (iii) FAST: our methodology applied to the problem defined in (13), which aims to identify solutions with the shortest possible travel time. (iv) PRACTICE: a conceivable baseline that mimics the human practice for driving an E-Truck. In particular, we first compute the fastest path from the origin to the destination without intermediary charging stops. We then simulate the E-Truck to drive at the fastest speed until the battery is below $tol = 20\%$ SoC. We then find and route to the nearest charging station and fully charge the battery. We repeat the process until the destination is reached. If we can not find a feasible solution, we restart the procedure with a larger $tol \leftarrow tol + 5\%$.

Runtime environment. We implement our approach in the Julia programming language[62] and run the simulation on the High-Performance Computing system CityU Burgundy with multiple computing nodes. Each node is equipped with two AMD EPYC 7742 64-core CPUs and 512 GB of memory. For each problem instance, we use 8 CPU cores and 16GB of memory to compute the solution with our approach.

Other parameters and implementation details. The number of charging stops N for the CARBON and ENERGY strategies is aligned with that of the FAST strategy. Under these typical conditions, the number of charging stops does not exceed 12. We configure the conservative lower bound ratio as $\alpha = 0.05$ and limit the maximum number of iterations to 100. For each origin-destination pair, the default deadline is defined as $T = 1.2T_f$, where T_f represents the minimum travel time determined by the FAST strategy. Additionally, we assume that the E-Truck begins its journey with its battery fully charged, i.e., $\beta_0 = B$. We assume the carbon intensity of the initial battery π_0 is the average carbon intensity at the origin on the start date. Therefore, for a trip without intermediary charging stops, the incurred carbon footprint is $(\beta_0 - \beta_d) \cdot \pi_0$, where β_d is the final battery SoC at the destination.

Data availability

All datasets generated and analyzed in this study are available in the accompanying Source Data files. The US network data[51], elevation data[52], origin-destination pairs data[13], charging station data[19], carbon intensity data[15], vehicle adoption data[14] are all publicly available. The road traffic data can be accessed through HERE Maps' API[20] and is subject to HERE Maps' terms of use. Source data are provided with this paper.

Code availability

The custom computer code used to generate results can be accessed through the GitHub repository[63].

References

1. Davis, S. C. & Boundy, R. G. *Transportation Energy Data Book: Edition 40*. Technical report (Oak Ridge National Lab. (ORNL) 2022).
2. Brown, A. L., Fleming, K. L. & Safford, H. R. Prospects for a highly electric road transportation sector in the USA. *Curr. Sustain./Renew. Energy Rep.* **7**, 84–93 (2020).
3. Borlaug, B. et al. Heavy-duty truck electrification and the impacts of depot charging on electricity distribution systems. *Nat. Energy* **6**, 673–682 (2021).
4. Muratori, M. et al. *U.S. National Blueprint for Transportation Decarbonization: A Joint Strategy to Transform Transportation*. Technical Report DOE/EE-2674, United States. Department of Energy. (Office of Energy Efficiency and Renewable Energy, 2023).

5. Deng, L., Hajiesmaili, M. H., Chen, M. & Zeng, H. Energy-efficient timely transportation of long-haul heavy-duty trucks. *IEEE Trans. Intell. Transp. Syst.* **19**, 2099–2113 (2017).
6. Liu, Q., Zeng, H. & Chen, M. Energy-efficient timely truck transportation for geographically-dispersed tasks. *IEEE Trans. Intell. Transp. Syst.* **21**, 5148–5159 (2020).
7. Baum, M., Dibbelt, J., Wagner, D. & Zündorf, T. Modeling and engineering constrained shortest path algorithms for battery electric vehicles. *Transp. Sci.* **54**, 1571–1600 (2020).
8. Strehler, M., Merting, S. ören & Schwan, C. Energy-efficient shortest routes for electric and hybrid vehicles. *Transp. Res. Part B Methodol.* **103**, 111–135 (2017).
9. Zhang, Y., Qu, X. & Tong, L. Optimal eco-driving control of autonomous and electric trucks in adaptation to highway topography: Energy minimization and battery life extension. *IEEE Trans. Transp. Electrif.* **8**, 2149–2163 (2022).
10. Hassin, R. Approximation schemes for the restricted shortest path problem. *Math. Oper. Res.* **17**, 36–42 (1992).
11. Crippa, M. et al. *GHG Emissions of All World Countries*. (KJ-NA-30831-EN-N (online),KJ-NA-30831-EN-C (print)), (Publications Office of the European Union, 2021).
12. Fernández, E., Leitner, M., Ljubić, I. & Ruthmair, M. Arc routing with electric vehicles: dynamic charging and speed-dependent energy consumption. *Transp. Sci.* **56**, 1219–1237 (2022).
13. Hwang, H.-L. et al. *The Freight Analysis Framework Verson 4 (FAF4)-Building The FAF4 Regional Database: Data Sources and Estimation Methodologies*. Technical Report ORNL/TM-2016/489 (Oak Ridge National Lab.(ORNL), 2016).
14. Ledna, C. et al. Assessing total cost of driving competitiveness of zero-emission trucks. *iScience* **27**, 109385 (2024).
15. Gagnon, P., Cowiestoll, B. & Schwarz, M. *Cambium 2022 Scenario Descriptions and Documentation*. Technical Report NREL/TP-6A40-84916 (National Renewable Energy Lab. (NREL), 2023).
16. Kerry, J. and McCarthy, G. *The Long-Term Strategy of the United States, Pathways to Net-Zero Greenhouse Gas Emissions by 2050* (The United States Department of State and the United States Executive Office of the President, 2021).
17. Budzianowski, W. M. Negative carbon intensity of renewable energy technologies involving biomass or carbon dioxide as inputs. *Renew. Sustain. Energy Rev.* **16**, 6507–6521 (2012).
18. Hanssen, S. V. et al. The climate change mitigation potential of bioenergy with carbon capture and storage. *Nat. Clim. Chang.* **10**, 1023–1029 (2020).
19. OpenStreetMap contributors. Planet dump retrieved from https://planet.osm.org. https://www.openstreetmap.org, (2017).
20. HERE Maps. Traffic flow using corridor in HERE maps. https://developer.here.com/api-explorer/rest/traffic/flow-using-corridor (2022).
21. Charge Point, Inc. Your EV charging platform of choice. https://www.chargepoint.com/ (2025).
22. PlugShare, LLc. PlugShare—EV Charging Station Map. https://www.plugshare.com/ (2025).
23. Electricity Maps. Carbon Intensity Data. https://electricitymaps.com/ (2024).
24. Alonso-Mora, J., Samaranayake, S., Wallar, A., Frazzoli, E. & Rus, D. On-demand high-capacity ride-sharing via dynamic trip-vehicle assignment. *Proc. Natl. Acad. Sci. USA* **114**, 462–467 (2017).
25. Kim, G., Ong, Yew-Soon, Heng, ChenKim, Tan, PuaySiew & Zhang, NengshengAllan City vehicle routing problem (city vrp): a review. *IEEE Trans. Intell. Transp. Syst.* **16**, 1654–1666 (2015).
26. Moghdani, R., Salimifard, K., Demir, E. & Benyettou, A. The green vehicle routing problem: a systematic literature review. *J. Clean. Prod.* **279**, 123691 (2021).
27. Dündar, H., Ömürgönülşen, M. & Soysal, M. A review on sustainable urban vehicle routing. *J. Clean. Prod.* **285**, 125444 (2021).
28. Su, J., Lin, Q. & Chen, M. Follow the sun and go with the wind: carbon footprint optimized timely e-truck transportation. In *Proc. 14th ACM International Conference on Future Energy Systems* 159–171 (Association for Computing Machinery (ACM), 2023).
29. Baum, M., Dibbelt, J., Gemsa, A., Wagner, D. & Zündorf, T. Shortest feasible paths with charging stops for battery electric vehicles. *Transp. Sci.* **53**, 1627–1655 (2019).
30. Boyd, S. & Vandenberghe, L. *Convex Optimization* (Cambridge University Press, 2004).
31. Montoya, A., Guéret, C., Mendoza, J. E. & Villegas, J. G. The electric vehicle routing problem with nonlinear charging function. *Transp. Res. Part B Methodol.* **103**, 87–110 (2017).
32. Zhang, W., Zhao, H. & Xu, M. Optimal operating strategy of short turning lines for the battery electric bus system. *Commun. Transp. Res.* **1**, 100023 (2021).
33. Maji, D., Sitaraman, R. K. & Shenoy, P. DACF: day-ahead carbon intensity forecasting of power grids using machine learning. In *Proc. Thirteenth ACM International Conference on Future Energy Systems* 188–192 (Association for Computing Machinery (ACM), 2022).
34. Su, J., Chen, M. & Zeng, H. Energy efficient timely transportation: a comparative study of internal combustion trucks and electric trucks. In *Proc. 8th ACM International Conference on Systems for Energy-Efficient Buildings, Cities, and Transportation* 224–225 (Association for Computing Machinery (ACM), 2021).
35. Hancock, M. W. & Wright, B. *A Policy on Geometric Design of Highways and Streets* Vol. 3, 20 (American Association of State Highway and Transportation Officials, 2013)..
36. Su, J., Lin, Q., Chen, M., and Zeng, H. Minimizing carbon footprint for timely e-truck transportation: hardness and approximation algorithm. In *Proc. 62nd IEEE Conference on Decision and Control* 7773–7778 (Institute of Electrical and Electronics Engineers (IEEE), 2023).
37. Su, J. et al. Minimizing emission for timely heavy-duty truck transportation. *IEEE Trans. Intell. Transp. Syst.* **26**, 1454–1469 (2025).
38. Boyd, S. & Mattingley, J. Branch and bound methods. *Notes for EE364b, Stanford University* 2006, 07 (2007).
39. Boyd, S., Xiao, L. & Mutapcic, A. Subgradient methods. *lecture notes of EE392o, Stanford University, Autumn Quarter* 2004, 2004–2005 (2003).
40. Bazaraa, M. S. & Sherali, H. D. On the choice of step size in subgradient optimization. *Eur. J. Oper. Res.* **7**, 380–388 (1981).
41. Camerini, P. M., Fratta, L., and Maffioli, F.. *On Improving Relaxation Methods by Modified Gradient Techniques* 26–34 (Springer Berlin Heidelberg, 1975).
42. Goel, A. & Kok, L. Truck driver scheduling in the United States. *Transp. Sci.* **46**, 317–326 (2012).
43. Mayerle, S. érgioFernando, De Genaro Chiroli, DaianeMaria, Neiva de Figueiredo, João & Rodrigues, HidelbrandoFerreira The long-haul full-load vehicle routing and truck driver scheduling problem with intermediate stops: an economic impact evaluation of brazilian policy. *Transp. Res. Part A Policy Pract.* **140**, 36–51 (2020).
44. Basso, R., Kulcsár, Balázs, Sanchez-Diaz, I. & Qu, X. Dynamic stochastic electric vehicle routing with safe reinforcement learning. *Transp. Res. Part E Logist. Transp. Rev.* **157**, 102496 (2022).
45. Maji, D., Shenoy, P. & Sitaraman, R. K. Carboncast: multi-day forecasting of grid carbon intensity. In *Proc. 9th ACM International Conference on Systems for Energy-Efficient Buildings, Cities, and Transportation* 198–207 (Association for Computing Machinery (ACM), 2022).
46. Madziel, M. Impact of weather conditions on energy consumption modeling for electric vehicles. *Energies* **18**, 1994 (2025).
47. Xu, W., Liu, Q., Chen, M. & Zeng, H. Ride the tide of traffic conditions: opportunistic driving improves energy efficiency of timely truck transportation. *IEEE Trans. Intell. Transp. Syst.* **24**, 4777–4793 (2023).

48. Speth, D., Plötz, P., Funke, S. & Vallarella, E. Public fast charging infrastructure for battery electric trucks–a model-based network for germany. *Environ. Res. Infrastruct. Sustain.* **2**, 025004 (2022).
49. Speth, D., Plötz, P. & Wietschel, M. An optimal capacity-constrained fast charging network for battery electric trucks in Germany. *Transp. Res. Part A Policy Pract.* **193**, 104383 (2025).
50. Karlsson, J. & Grauers, A. Agent-based investigation of charger queues and utilization of public chargers for electric long-haul trucks. *Energies* **16**, 4704 (2023).
51. Teresco, J. Map-based Educational Tools for Algorithm Learning (METAL) project. https://courses.teresco.org/metal/ (2022).
52. Farr, T. G. et al. The shuttle radar topography mission. *Rev. Geophys.* **45**, RG2004 (2007).
53. Gonder, J. D., Brooker, A. D., Wood, E. W. & Moniot, M. *Future Automotive Systems Technology Simulator (Fastsim) Validation Report*. Technical Report NREL/TP-5400-81097 (National Renewable Energy Lab.(NREL) 2021).
54. Tesla. Tesla Semi official website. Accessed 14 March 2022. https://www.tesla.com/semi (2022).
55. Powell, B., Johnson, C., Yip, A. & Snelling, A. *Electric Medium-and Heavy-Duty Vehicle Charging Infrastructure Attributes And Development*. Technical Report NREL/TP-5R00-91571 (National Renewable Energy Laboratory (NREL), 2024).
56. Nykvist, Björn & Olsson, O. The feasibility of heavy battery electric trucks. *Joule* **5**, 901–913 (2021).
57. Kenworth. Kenworth t800, accessed 25 May 2021. https://www.kenworth.com/trucks/t800(2021).
58. U.S. Energy Information Administration. Carbon Dioxide Emissions Coefficients. Accessed 14 March 2022. https://www.eia.gov/environment/emissions/co2_vol_mass.php (2022).
59. Hoehne, C. et al. Exploring decarbonization pathways for USA passenger and freight mobility. *Nat. Commun.* **14**, 6913 (2023).
60. Kumar, S. S. & Himabindu, V. J. M. Sf. E. T. Hydrogen production by PEM water electrolysis–a review. *Mater. Sci. Energy Technol.* **2**, 442–454 (2019).
61. Islam, E. et al. *Detailed Simulation Study to Evaluate Future Transportation Decarbonization Potential*. Technical Report ANL/TAPS-23/3 (Argonne National Laboratory (ANL), 2023).
62. Bezanson, J., Edelman, A., Karpinski, S. & Shah, V. B. Julia: a fresh approach to numerical computing. *SIAM Rev.* **59**, 65–98 (2017).
63. Su, J., Lin, Q. & Minghua, C. Optimizing carbon footprint in long-haul heavy-duty e-truck transportation, https://github.com/sujunyan/cfo, https://doi.org/10.5281/zenodo.16758048 (2025).
64. U.S. Energy Information Administration. May 2023 monthly energy review. Technical report, DOE/EIA-0035(2023/5) (U.E. Energy Information Administration, 2023).

Acknowledgements

Part of this work has been presented in ACM e-Energy'23[28]. This work was carried out using the computational facilities, CityU Burgundy, managed and provided by the Computing Services Centre at City University of Hong Kong (https://www.cityu.edu.hk/). This work is supported in part by a General Research Fund from Research Grants Council, Hong Kong (Project No. 11200124) (M.C.), a Collaborative Research Fund from Research Grants Council, Hong Kong (Project No. C1049-24G) (M.C.), an InnoHK initiative, The Government of the HKSAR, Laboratory for AI-Powered Financial Technologies, a Shenzhen-Hong Kong-Macau Science & Technology Project (Category C, Project No. SGDX20220530111203026) (M.C.), and a Start-up Research Grant from The Chinese University of Hong Kong, Shenzhen (Project No. UDF01004086) (M.C.).

Author contributions

M.C. conceived the study. J.S. collected the data for motivation and experiments. J.S. and M.C. developed the formulation. J.S., Q.L., and M.C. developed the algorithm. J.S. conducted the experiments. J.S. and M.C. analyzed the algorithm performance and experimental results. J.S., Q.L. and M.C. wrote and improved the manuscript. All of the authors discussed the formulation, the algorithm, and the results, as well as reviewed the manuscript.

Competing interests

The authors declare no competing interests.

Additional information

Supplementary information The online version contains supplementary material available at https://doi.org/10.1038/s41467-025-64792-2.

Correspondence and requests for materials should be addressed to Minghua Chen.

Peer review information *Nature Communications* thanks Patrick Plotz, Xiaobo Qu and the other, anonymous, reviewer(s) for their contribution to the peer review of this work. A peer review file is available.